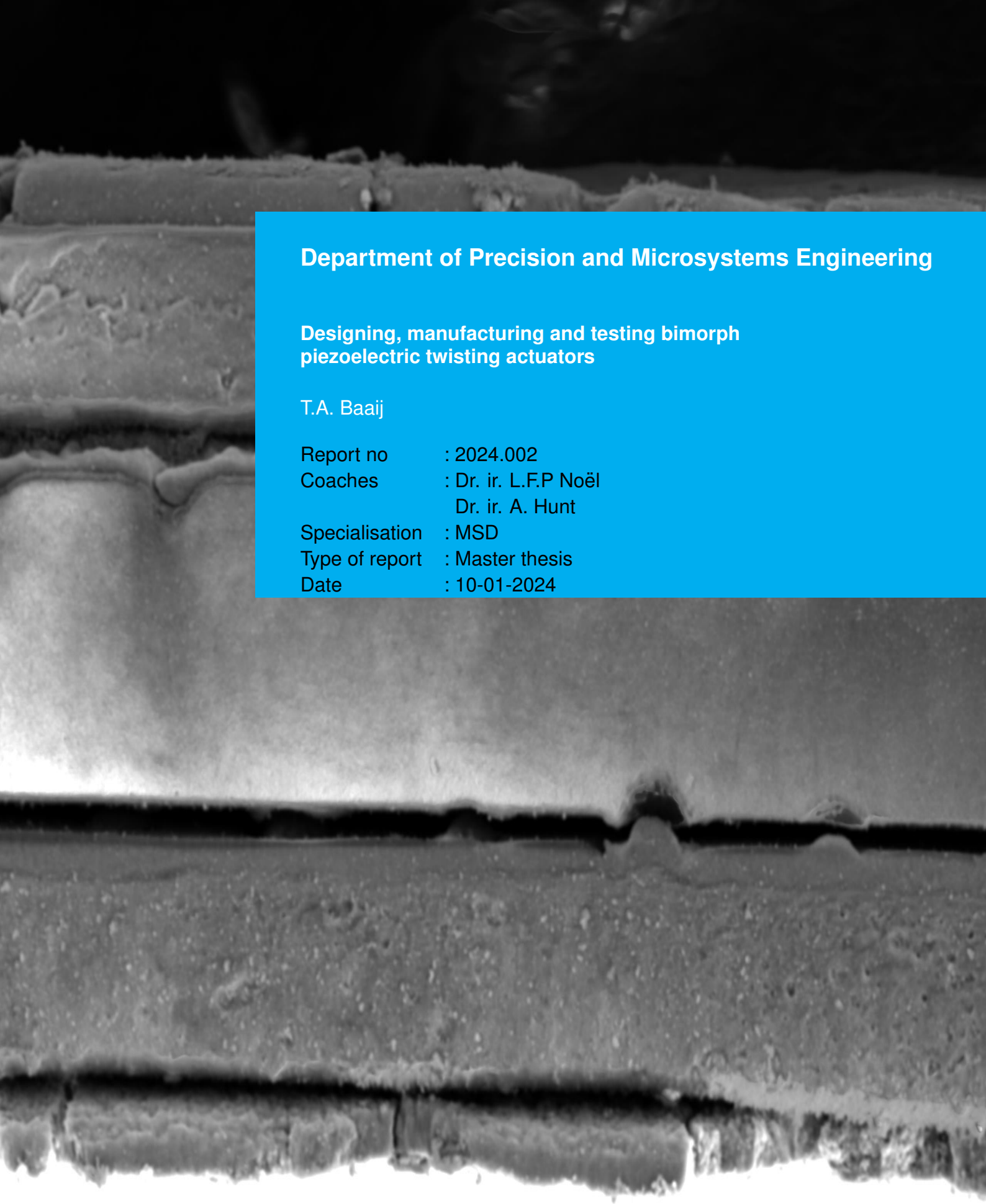

Department of Precision and Microsystems Engineering

Designing, manufacturing and testing bimorph piezoelectric twisting actuators

T.A. Baaij

Report no : 2024.002
Coaches : Dr. ir. L.F.P Noël
Dr. ir. A. Hunt
Specialisation : MSD
Type of report : Master thesis
Date : 10-01-2024

TU Delft Delft University of Technology

Challenge the future

Designing, manufacturing and testing bimorph piezoelectric twisting actuators

by

T.A. Baaij

to obtain the degree of Master of Science
at the Delft University of Technology,
to be defended publicly on Wednesday January 10, 2024 at 13:00.

Student number: 4681398
Thesis committee: Dr. ir. L.F.P Nol, TU Delft, supervisor
Dr. ir. A. Hunt, TU Delft, supervisor
Dr. J. Yang, TU Delft

TU Delft

Contents

1 Abstract

This thesis report contains two papers. The first paper is a literature study on mechanisms, smart actuated materials and controllable joints. In this paper, several smart materials are identified and it is discussed how they can be embedded in different mechanisms. From this paper, it is concluded that fast-response smart material twisting actuators do currently not exist. The second paper studies the design and development of such an actuator. The study presents a design and manufacturing methodology of a planer actuator that generates out-of-plane rotation. It first investigates different out-of-plane deformation modes and how they can be used to achieve the desired motion. Based on an analytical model on the shape morphing of piezoelectric macro fibre composites, a methodology is developed to generate out-of-plane twisting deformation. This concept is used to design a carbon black electrode pattern, which can be spray-deposited on a kapton substrate. This electrode is subsequently used to selectively actuate parts of a P(VDF-TrFE- CTFE) polymer layer. The selective stimulation of the layer results in the desired twisting deformation. This study demonstrates how flat designs can be laminated in a planar additive manufacturing process to induce complex 3D motion. The spray-deposition process was capable of manufacturing bimorph actuators with a 1.6mm resolution. The resulting actuators have a length of 41mm and a width of 10 to 20mm and a thickness of 120 to 139μm. The experiments are used to characterize the effect of the design parameters such as actuator width and thickness on the magnitude of the deformation. As theorized in the analytical model, the thinner more slender samples show the largest rotation which is measured to rotate up to 3.38 degrees. From the experiments it is also found that thinner samples show dielectric breakdown at much lower voltages, around 100V, compared to thicker samples from the same design that performed up to 480V. The study also investigates the quality of the deformation of the actuators, i.e. pure twisting or a combination of twisting and bending deformation. It is verified that uneven layers or asymmetric actuators show significant unimorph bending behaviour, with displacements up to 1.5mm while rotating 3.38 degrees. To the author's best knowledge, this study presents the first working prototypes of fast-response smart material twisting actuators.

2 Mechanisms, smart actuated materials and design methods for compact, controllable, compliant joints

Literature survey

Mechanisms, smart actuated materials and design methods for compact, controllable, compliant joints

Baaij, T. A.
Department of Precision and Microsystems Engineering
Delft University of Technology
Delft, Netherlands
t.a.baaij@student.tudelft.nl

***Abstract*—Smart actuated materials can be used to induce deformations. These deformation can significantly change the position or geometry of a mechanism to adapt to their surroundings and applications. Mechanisms that can actively change their geometry have applications in small scale robotics and high-tech mechanisms. For example, they can be used to create shape-morphing wings or locomoting robots. Embedding smart materials directly in a mechanism, makes it more compact and lowers the amount of material and energy required to manufacture and operate the mechanism. As a result, the mechanism becomes more efficient and more sustainable. This study reviews different mechanisms that can be used in controllable joints. We identify a lamina emergent torsional joint that complies with rotational motion. This passive joint is a sub-part of a lamina emergent mechanism which transforms from a planar initial state, into a 3D geometry. The planar initial state allows for planar manufacturing processes, which is advantageous for small scale mechanisms. We propose to embed a smart actuated material in this joint to develop a compact, compliant, controllable hinge. After reviewing different smart active materials, we propose to use a piezoelectric composite to deform the joint. This composite allows for a high bandwith and accurate control of the joint. FEM is suggested to model the electro-mechanical behaviour of the composite. This FEM can subsequently be used in a two-phase MMC, density-based optimization study to optimize the size, shape and polarization direction of the active elements in their host-structure.**

I. Introduction

Scaling down mechanisms can improve their performance and lower their power consumption. Smaller parts have a lower mass which can result in faster and more efficient operation with a lower energy input. Thus, miniaturized mechanisms are more sustainable with better performance. Miniaturisation can be applied to advance many engineering fields such as robotics, minimally invasive surgery or high-tech industries.

To meet the increasing innovation is these fields, researchers are devoting significant effort to study and develop smart material actuators. Smart material actuators can convert energy from one physical domain to another. For example, thermal energy can be used to impose a strain on a material, thus converting thermal energy to mechanical energy. The embedding of smart material actuators can result in miniaturization of robots or steerable endoscopes by replacing mechanical actuators with smart active materials.

Mechanical actuators displace parts of the mechanism to induce the desired deformation. These moving parts cause friction, which will become considerably large on small scales. Thus, the mechanism need a significant amount of energy to overcome this friction. Smart material actuators can be embedded in the material of the mechanism. This eliminates the parts that cause friction as the movement is generated by deforming the structure of the mechanism directly.

This study reviews compact, compliant hinging mechanisms, smart material actuators and their modelling and design approaches. In Sec. II, we focus on planar mechanisms that can undergo out-of-plane bending or hinging. The main benefit of planar mechanisms is that they can undergo planar manufacturing processes. This is advantageous to manufacture the mechanisms on small scales. We identify four different mechanisms; uni-and bimorph, lamina emergent mechanisms (LEMs), origami and kirigami (O&K) and wires in Subsecs II-A, II-B, II-C and II-D respectively. First, we briefly discuss the principles behind the mechanisms. Subsequently, we provide practical examples on how these mechanisms can be utilised. We aim to qualify the performance of each mechanism, i.e., what are the maximum bending angles and are the mechanisms suitable for miniaturization by embedding active materials in their structures. A comparative overview of the discussed mechanisms is presented in Subsec. V-A. We also discuss alternative applications for these mechanisms.

In Sec. III, we review smart material actuators and their respective stimuli. Here, we focus on existing practical implementations. We review different actuating stimuli such as heat, light, magnetic and electric fields. For each category of smart materials, we start with the physical principles that explain the material's behaviour. Subsequently, we show practical implementations of the materials and we discuss their strengths and weaknesses. In Subsec. V-B we present our main findings and we discuss what materials are suitable for controllable compliant hinges and why.

In Sec. IV, we look into modelling and design approaches that can be applied to smart actuated compliant joints. First, we review different modelling and design methods specifically for the different discussed mechanisms in Subsec. IV-A. Subsequently, we discuss what modelling and design approaches are available for the most common smart material actuation in Subsec. IV-B; thermal and electric. Subsection V-C, discusses how these approaches can be utilised to model the actuated hinge and optimize its performance.

II. Compliant bending mechanisms

This section provides an overview of different compliant mechanisms that rely on shape-deformation to morph their structure into the desired geometry or achieve bending. Unimorph and bimorph bending and LEMs are discussed in Subsecs. II-A and II-B respectively. These mechanisms deform their structure to achieve the desired shape-shifting. They use elongation, contraction or twisting to create out-of-plane deformation. This elastic deformation can be used to generate hinge-like behaviour. Other mechanisms such as O&K, described in Subsec. II-C, cleverly fold and bend material to morph 2D surfaces into 3D geometries. The ideas behind their 2D to 3D transformation can be used in hinge-like mechanisms similar to LEMs. Other O&K patterns or tessellations show potential to be integrated in an active mechanical metamaterial (AMM) lattice. This lattice is built up from a repetition of unit cells. In each unit cell, small changes in property can be generated. For example, inducing a small rotation in each unit cell will lead to a large net change in surface curvature. Finally, wired mechanisms are reviewed in Subsec. II-D. Pulling on wires attached to a part of a mechanism that is partially constricted can bend the mechanism into the desired angle. The discussed mechanisms are compared in the conclusion.

A. Unimorph and bimorph bending

A mechanism is considered *unimorph* if it consists of an active and a passive layer and *bimorph* if it consists of two active layers. The bending can be generated by inducing elongation in the active layer, while its deformation is partially being constrained by the passive or the other active layer. The relative strain difference causes a bending moment around the effective neutral of the two layers. As a result, the material can bend up or down out-of-plane. The larger the strain difference between the layers, the sharper the bending angle. This principle can be used to transform any elongating or contracting motion, e.g., photostriction (Subsec. III-B) or magnetostriction (Subsec. III-C), into bending as shown in Fig. 1.

Fig. 1. Bending caused by induced strain differences

B. Lamina emergent mechanisms

LEMs create mechanisms that can emerge out of planar materials. To do so, LEMs are composed of elements that support and comply with out-of-plane bending motions which are usually passive. However, it might be possible to actuated LEMs to generate active, hinge-like mechanisms. LEMs are manufactured from planar materials and work with compliant elements that can deform out of the fabrication plane. Due to their planar initial state, they are compact and can be manufactured with stamping and cutting. These methods are more difficult on 3D structures [32]. This makes LEMs excellent candidates for micro and macro applications. However, LEMs are difficult to model due to their large, often non-linear deformation. The designer also needs to account for singularity points, as inputs may result in several possible ranges of motion.

To accommodate for large out-of-plane bending angles, LEMs require suitable joints that can cope with the large angular rotation. Jacobsen et al. [33] proposed a lamina emergent torsional (LET) joint which is capable of reaching large bending angles, see Fig. 2. A centimeter-scale variant of this joint made of beryllium bronze, analyzed in [67], is reported to have a rotation angle of up to 54°. The mechanism does however suffer from off-axis flexibility, i.e., compression and tension at the joint.

Fig. 2. Links connected by LET joints, retrieved from [33]

Xie et al. [67] proposed a similar approach to an outside-deployed lamina emergent joint (OD-LEJ), see Fig. 3. Here, a bending angle of 170° is reached solely by elastic deformation in the mechanisms. The researchers report that the hinge is not suitable for high compression or tensions loads. Furthermore, the center of rotation moves significantly for higher bending angles which may not be desirable. However, large bending angles might be suitable as joints in locomoting small scale robots.

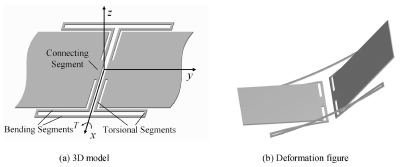

Fig. 3. OD-LEJ joint, retrieved from [67]

To counter the inherent flexibility of the compliant joints, Ma et al. [44] studied double laminated LET joints, as shown in Fig. 4. By laminating the joint with an aluminium foil layer, a similar bending stiffness in the joint is achieved while significantly increasing its tensile stiffness. It was reported that the laminating was successful for up to two in series connected joints. However, when adding a third joint (double laminated triple LET joints) it became vulnerable to delamination.

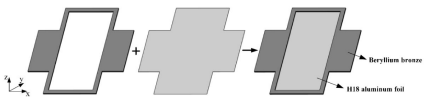

Fig. 4. Laminated LET joint, retrieved from [44]

C. Origami and kirigami inspired folding

Origami is the ancient Japanese art of folding paper to transform flat sheets into complex 3D geometries. Kirigami is a variation that also allows cutting of the sheets. Similar to LEMs, O&K structures benefit from a flat initial state that allows planar manufacturing processes. Using O&K, complex bends and curves can be realized. Peraza Hernandez et al. [26] proposed a method to turn complex curved geometries into polyhedral surfaces. These surfaces approximate the desired geometry closely when folded but can be unfolded and constructed from flat sheets.

Similarly, Lang and Howell [43] developed a methodology to generate rigidly foldable quadrilateral meshes. These meshes can morph from the flat to the deployed state. Fig. 5 shows a flat surface which can fold into a tubular construction demonstrating that the method can generate complex out-of-plane geometries by using a finite number of rotations over crease lines. Since the method constructs mechanisms with a single DOF, the entire mesh can be actuated with a single actuator instead of embedding actuation in every fold. The research does not illustrate how the meshes could be actuated, but it claims that a single compression force can fully deploy the mechanism.

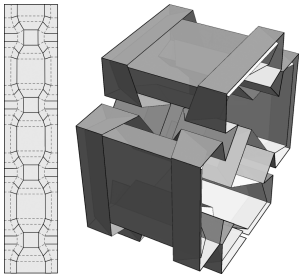

Fig. 5. Quadrilateral mesh and deployed state, retrieved from [43].

Chen et al. [11] developed a similar O&K inspired mesh to actively deploy a solar panel array. The researchers used shape memory polymers to deploy, i.e., unfold, the array as shown in Fig. 6. Since the shape-shifting is actuated, it might be possible that a similar approach can be used to create an actuated out-of-plane bending quadrilateral mesh. Shape memory polymers are reviewed in more detail in Subsec. III-F.

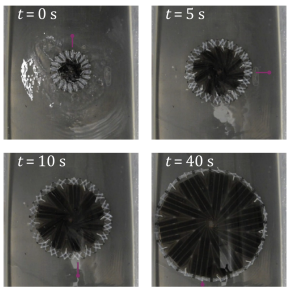

Fig. 6. Deployment of solar array, retrieved from [11]

Another way to limit the amount of actuators needed to deploy O&K mechanisms is proposed by Bhovad et al. [3]. The study embedded multi-stabilty in a robotic O&K skeleton. The researchers used two bistable Kresling origami segments. They have actuation cycles and can jump into different states changing their length, see Fig. 7. Utilising the jumps between the stable states, a peristaltic moving robot is created.

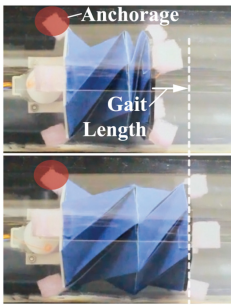

Fig. 7. Peristaltic moving robot, retrieved from [3]

A similar multi-stable approach was used by Overvelde et al. [29] to create bistable, folding hinges as shown in Fig. 8.

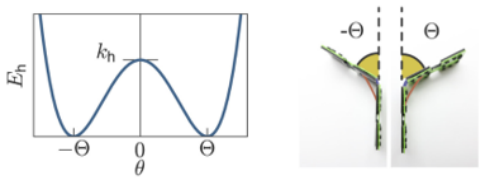

Fig. 8. Energy of bistable double well potential hinge, retrieved from [29]

Bistable solutions are very convenient since small perturbations will not compromise the behaviour or state of the system. However, they do not allow for continuous change in configuration. For the hinge in Fig. 8, this means that all bending angles between the stable points are dynamic translations between the discrete stable states. In other words, they are not statically reachable.

O&K mechanisms can also be used to construct a mechanism around other actuators. Felton et al. [17] embedded a self-folding origami structure with electronics. Using a shape memory composite, the flat sheet can fold itself autonomously into a crawling robot in four minutes. With the embedded electronics, the robot can subsequently crawl forward.

The above mentioned examples mainly exhibit unidirectional deployment, i.e., the mechanisms are flat or completely folded to a fixed predetermined shape. To construct a mechanism that allows continuous deformation in multiple directions, one could consider O&K tessellations. Tessellations consist of a lattice, or are built from the repetition of unit cells. Examples of these tessellations are miura-ori, which can fold/unfold, and Resch and waterbomb tessellations, which can additionally twist [8]. These mechanisms are shown in Figs. 9 and 10. By changing the amount of folding or bending in the different unit cells, the mechanisms allow continuous deformation.

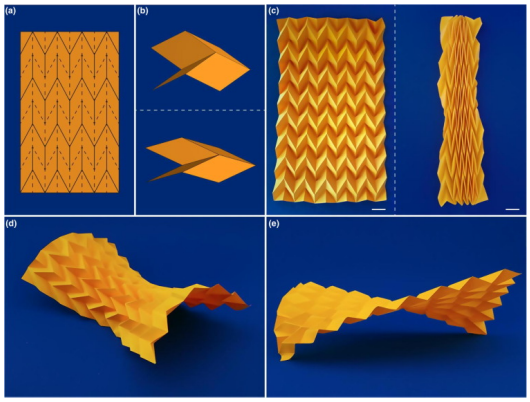

Fig. 9. Miura-ori tesselation, retrieved from [8]

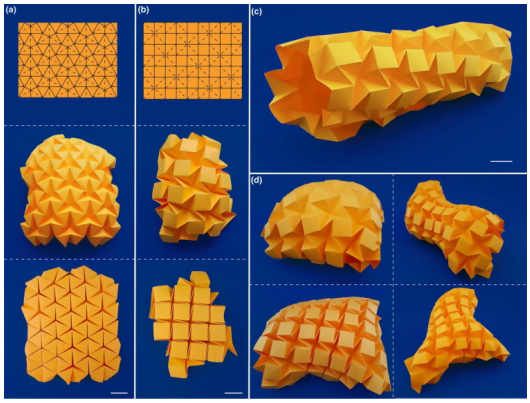

Fig. 10. Resch and waterbomb tessellations, retrieved from [8]

Embedding actuation in the unit cells of the tessellations turns the mechanism into an AMM that has an adapting surface curvature. These tessellations contain many DOFs. However, not all of them need to be actuated as shown for miura-ori sheets by Grey et al. [22]. This can significantly lowers the amount of actuators required to create multipurpose curvature-morphing materials. Yu et al. [68] studied how different geometries and curvatures could be folded from Resch patterns. The researchers investigated the nature of the folding and unfolding of the tessellation by looking at the energy stored in the creases.

D. Wires

The pulling of wires can bring parts of a mechanism closer together. This can result into the object bending into the desired direction. The mechanism that pulls on or twists the wires, is considered the actuation of the mechanism. The structure of the mechanism, translates the actuation into the desired motion. Neville et al. [47] worked on an actuated honeycomb structure based on a O&K inspired manufacturing process. Here, the structure of the mechanism translates the tension in the wires into bending. The experiments show that the structure can reach large bending angles, see Fig. 11.

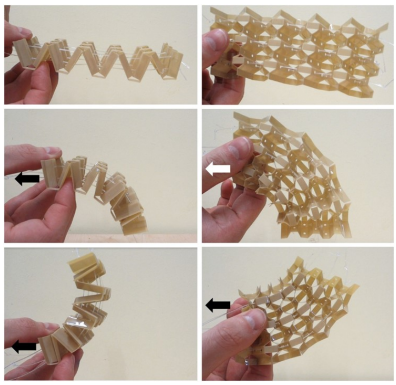

Fig. 11. Actuated honeycomb structure, retrieved from [47]

The effective length of wires can easily be shortened by twisting them together. Shomam et al. [56] proposed a simple linear actuator using this principle. Twisted string actuators (TSAs) behave like artifical muscles and can generate large bending angles [6]. TSAs can be implemented in hand-like grippers capable of complex gripping manipulation [40], see Fig. 12. However, such large deformations are difficult to model as they induce geometric nonlinearities. The twisting of the wires is proven to work on cm-scale devices. However, when miniaturising the system, the friction between the wires can become significant with respect to the output forces of the mechanism.

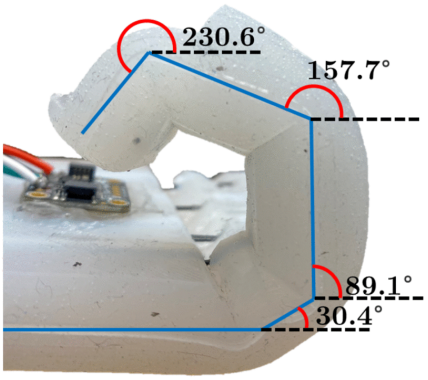

Fig. 12. Actuated TSA gripper, retrieved from [40]

III. Smart material actuators

This section explores smart material actuators. First, we consider pre-programmed materials in Subsec. III-A. Here, we look at materials that can deform from internal, residual stresses. These can for example be generated in a material by curing-induced stress, which results in the structure deforming. We also consider several external stimuli, such as light (Subsec. III-B) or magnetic fields (Subsec. III-C). Other active materials can be stimulated by locally applying an electric potential or Joule heating. These stimuli are common in piezoelectrics and shape memory materials, as described in Subsecs. III-F and III-G, respectively. For each category of smart material actuators, we first describe the physical working principle of the material. Subsequently, we provides examples of practical implementations of the material. This section aims to identify the strengths and weaknesses of the different materials. This can assist in selecting, or creating a suitable material for new applications.

A. Pre-applied stress

Residual stress in a material can induce bending which is undesired in most production processes. However, residual stress can also be exploited when applied deliberately. Sundaram et al. [59] proposed a method to 3D print self-folding electronics. During the printing process, UV light induces a swelling in the printed polymers which results in a strain within the composite. The physical principles behind this phenomenon are explained in Subsec. III-B. The methodology of purposely introducing a residual strain in a material are not limited to stimulation by light. This can be done using any other stimulant, such as heat, as well. After the manufacturing process, the work piece is lifted off the print bed and self-folds into the desired shape due to residual stress, see Fig. 13. Experiments show that complex 3D shapes can be created with embedded electronics that remain functional after the shape-shifting. The method results in large bending angles up to 100°. However, this is only achieved long after (≈1200 minutes) removing the initial constraints. The method is suitable for creating complex shapes with large bending angles with embedded components. However, the folding of the material is an irreversible process.

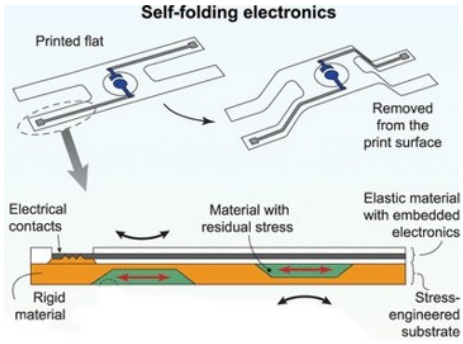

Fig. 13. Self folding electronics, retrieved and modified from [59]

B. Light induced bending

Mechanical strain can be induced by external light sources through different principles. Photostrictive materials are characterized by physical properties that cause the material to directly convert optical energy to mechanical strain. This principle has been extensively reviewed by Chen and Yi [10]. Other materials can convert optical energy to thermal energy. The produced heat can lead to an inhomogeneous strain distribution which causes the material to bend.

1) Photostriction: Photostriction is the light-induced-nonthermal dimensional change of a material and can be found in, for example, organic polymers and ferroelectric materials [41]. In organic polymers, light can reorient the molecular structure or cause ionization reactions. As a result, volumetric changes up to 400% can be induced. Furthermore, ferroelectric materials exhibit a bulk photovoltaic effect which results in a converse piezoelectric effect. Examples and more detailed explanations on the piezoelectric effect can be found under the subsection Subsec. III-G.

Similar to [59] from Fig. 13, Zhao et al. [73] induced a photostrictive effect during the curing of a liquid resin to create self-folding origami structures as shown in Fig. 14. The researchers irradiated the liquid resin with different light patterns during the curing. A photoabsorbing element in the resin leads to a nonuniform stress distribution along the thickness direction. When the resin is cured and taken off the manufacturing platform, the residual stress bends the material into the designed state. The bending takes approximately ten seconds and is irreversible.

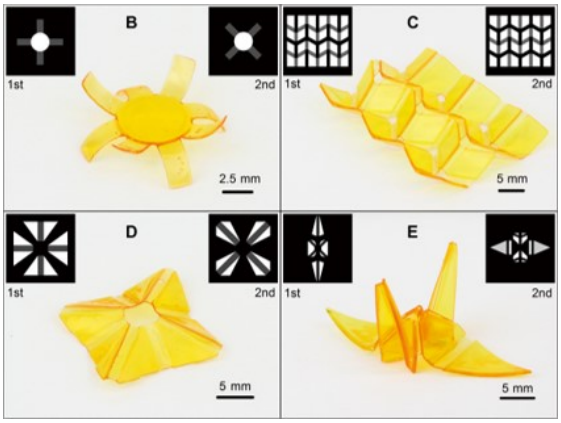

Fig. 14. Photostriction by photopolymerization, retrieved from [73]

2) Optical to thermal energy: The conversion of optical to thermal energy is applied by Torras et al. [61]. The researchers use liquid crystal elastomers with carbon embedded nanotubes that bend when irradiated. The radiation generates heat resulting in an inhomogeneous strain distribution. The material shows short response time (≈4s) but the generated heat might not be desired in all situation. The heat can affect the mechanism surrounding the active material. The experiment is shown in Fig. 15.

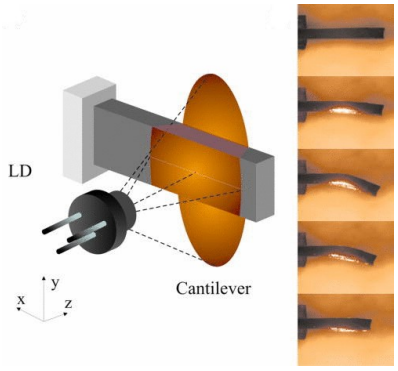

Fig. 15. Irradiated bending cantilever beam, retrieved from [61]

C. Magnetic

Bending, elongating and twisting can also be induced by applying a magnetic field. Several different mechanisms such as embedding ferromagnetic fibres and magnetostriction are already investigated and implemented. There are also magnetic shape memory alloys where a shape memory effect is stimulated by a magnetic field which is reviewed in more detail in Subsec. III-F2.

1) Nickel-coated carbon fibres: Stanier et al. [58] aligned Nickel-coated Carbon Fibres (NiCF) in a host matrix where the fibres could be manipulated by an external magnetic field to induce bending or twisting, see Fig. 16. The paper proposes a manufacturing process which successfully aligns the fibres in the desired direction with an inexpensive setup. With a low magnetic field (< 0.2T) bending or twisting angles up to 25° are achieved. The research shows that there are critical bending or twisting angles where the sample deformation becomes unstable. As the magnetic field passes the critical angle a sudden increase in the actuation angle is observed. This could make it difficult to accurately manipulate the fibres into the desired angle when it lies close to the critical angle. Activate multiple bends in different directions remains challenging as several interfering magnetic fields will be required.

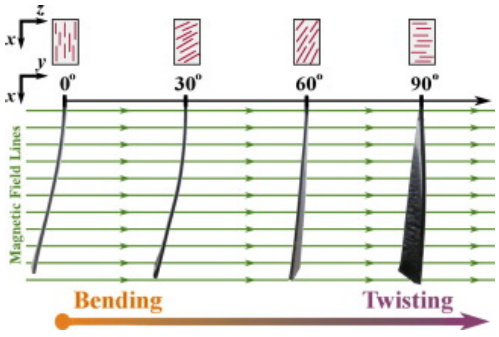

Fig. 16. Bending and twisting of matrix embedded with NiCF, retrieved from [58]

2) Magnetostriction: Magnetic fields can also change the shape of materials by rotating small magnetic domains. Magnetostrictive behaviour can elongate and shorten the material based on the direction of the applied magnetic field, making it a reversible process. Magnetostrictive materials (MSMs) can elongate approximately 0.2%. MSMs are capable or producing large blocking forces, operate on a large bandwith [48] and are already successfully implemented in 2D lattices where in-plane deformations are induced without contact [57]. The lattice unit cell deformation under a magnetic field is shown in Fig. 17. Stimulating the deformation with an external magnetic field does not allow for local control of the deformations. The applied field exerts influence on all neighbouring unit cells and interferes with other magnetic fields.

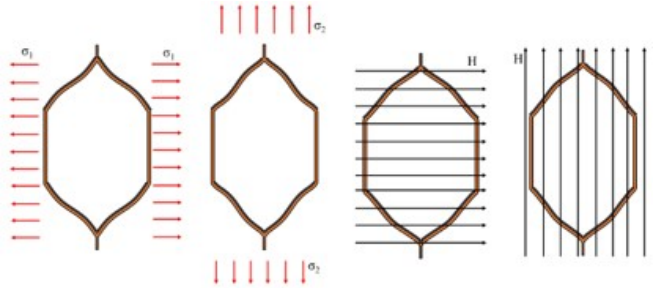

(a) Deformation under the effect of externally applied stress σ_1 in direction 1.
(b) Deformation under the effect of externally applied stress σ_2 in direction 2.
(c) Deformation under the application of externally applied magnetic field in horizontal direction.
(d) Deformation under the application of externally applied magnetic field in vertical direction.

Fig. 17. Magnetostrictive 2D lattice and its deformation, retrieved from [57]

D. Hydrogels

Hydrogels can be synthesized to have different deforming capabilities that can be stimulated by temperature, light and pH [30, 51]. The stimuli induce a swelling in the hydrogels which results in a mechanical strain. Combining elongating and contracting hydrogels will produce bending or twisting behaviour [34]. Certain hydrogels have shape memory effects that are triggered by surrounding solutions [1]. Hydrogels can undergo large volumetric changes, but are often limited by their response time. It can take several hours, for centimeter-scale hydrogels to fully deform [30]. Bidirectional deforming hydrogels are known as smart-hydrogels. An example of a light stimulated hydrogel, can be seen in Fig. 18 by Park et al. [50]. Here, the material folds under influence of a laser. The folding and relaxation of the material causes a forward locomotion.

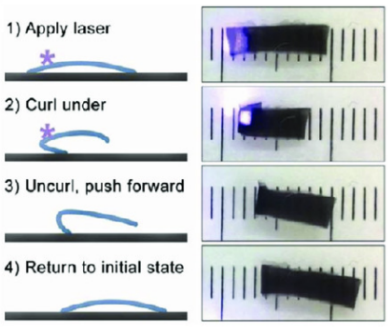

Fig. 18. Hydrogel locomotor, retrieved from [50]

E. Pneumatic

Pneumatically inflating parts of the material can cause bending which is used in several applications such as soft robotics and compliant grippers. Wang et al. [62] created and experimentally tested soft compliant grippers. The paper shows a very large bending angle (≈165°), see Fig. 19. Similarly, Katugampala et al. [39] integrated pneumatically inflated chambers around a soft, bendable skeleton. When the chambers are deflated, the robot can bend into several different directions. Pneumatically actuated materials can achieve large bending angles. When the deformation of a soft body is blocked by external interference, an increasingly applied pressure does not result in additional deformation. This makes the control over the direction and degree of bending often difficult. Additionally, pneumatically deformed soft bodies undergo many nonlinear deformations.

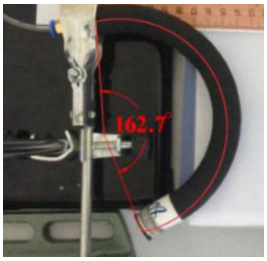

Fig. 19. Large bending of pneumatic gripper, retrieved from [62]

F. Shape memory materials

Shape memory materials are materials that can be deformed and return to their original geometry when subjected to specific stimuli [28]. Most shape memory materials are stimulated by heat, but there are exceptions as shown in Subsec. III-F2. This subsection covers the differences and existing applications of shape memory alloys (SMAs), ferromagnetic shape memory alloys (FSMAs) and shape memory polymers (SMPs).

1) Shape memory alloys: SMAs have a designed geometric shape which, after deformation, can be recovered by heat. The alloys crystalline structure can be in three different phases: twinned martensite, detwinned martensite, and austenite. When the twinned martensite phase is subjected to a load, the resulting deformation is manifested in the structure of the crystal and the martensite phase becomes detwinned. Upon heating, the detwinned martensite phase enters the austenite phase. This restructures the crystal and after cooling the original geometry (in the twinned martensite phase) is recovered. The shape memory effect is show in Fig. 20. The response time of SMAs is limited to their ability to dissipate the heat to recover their original shape. They operate on specific temperatures, which might not be suitable for all applications

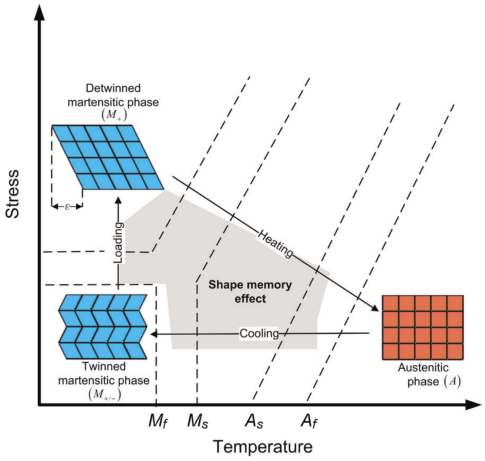

Fig. 20. Shape memory effect, retrieved from [12]

Hawkes et al. [25] used this phenomenon to create a self-folding material. Electrical wires deliver thermal energy (Joule heating) to the SMAs causing the material to fold. Subsequently, embedded magnets snap together to completely fold the material together. With this method, it is possible to individually trigger folds at the desired location and this was used to fold the material into aeroplanes and boats. However, due to the use of permanent magnets, the folding was unidirectional. Figure 21 shows a timelapse of the folding the SMA hinges to create an aeroplane shape. Here it is clearly demonstrated that each fold can be actuated individually.

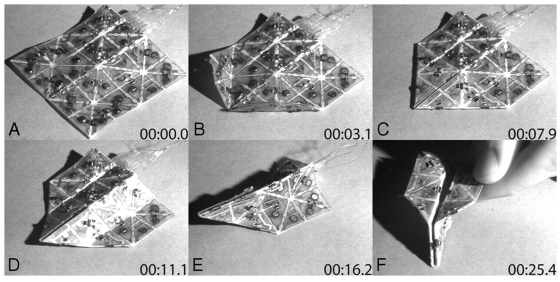

Fig. 21. SMA aeroplane folding, retrieved from [25]

Firouzeh et al. [18] proposed a similar approach, using multiple hinges. Here, a large bending angle up to 150° can be achieved. A robot with four legs is created, see Fig. 22. Each leg contains two mirrored unidirectional SMA hinges which can stretch and fold the leg. By controlling the movement of each leg separately, the robot is able to crawl.

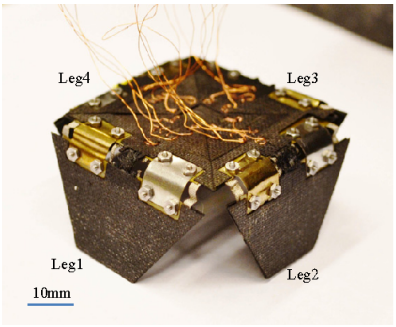

Fig. 22. SMA crawling robot, retrieved from [18]

Boyvat et al. [7] implemented SMA coils that are actuated by a magnetic field close to the coils resonance frequency. The resonating generates heat, causing the coils to alter their shape and bend the material. Here, multiple coils with different resonant frequencies are implemented that can be controlled individually. The coils and robot are shown in Fig. 23.

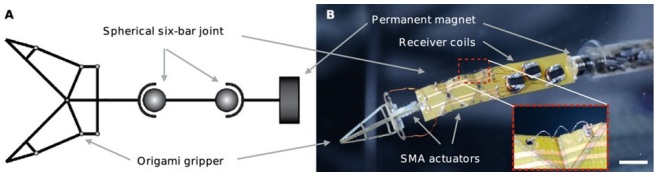

Fig. 23. SMA folding joint robot, retrieved from [7]

Wang et al. [64] embedded a SMA wire to create actuated hinges in a soft gripper, see Fig. 24. The extension of the wire would fold the soft compliant gripper to grab and lift objects. To delicately hold and handle an object, the compliant nature of these hinges is favoured. However, the flexible hinge might not be desired in situations where the hinge needs to be fixed in position.

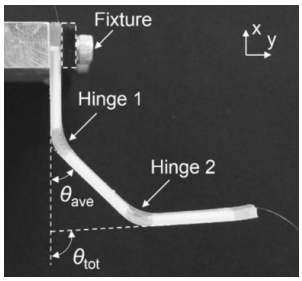

Fig. 24. SMA gripper, retrieved from [64]

2) Ferromagnetic shape memory alloys: FSMAs are stimulated by a magnetic field instead of heat. There are two ways to generate large strains based on the type of alloy used. The first, magnetically induced austenite, is based on the magnetocaloric effect. Here, a magnetic field induces a phase transformation from the martensite to the austenite phase. The second, magnetically induced reorientation, keeps the ferromagnetic material in the martensite phase but switches into variants in the martensite phase that favour the orientation of the applied magnetic field [16]. FSMAs can elongate up to 6% [42], which is much larger than MSMs. However, the alloys provide a relatively low blocking force. The strain of FSMAs is 60 times larger than piezoelectric materials such as Lead Zirconate Titanate (PZT), but have a similar work output.

3) Shape memory polymers: SMPs can deform when they are stimulated by light, moisture or pH change. However, the most common stimulus is heat. SMPs are lightweight compared to SMAs and FSMAs and are more bio-compatible. The molecular structure of SMPs it heated to a highly elastic state. In this state, the molecular chains can be stretched and displaced. Lowering the temperature locks the molecular chains in their deformed positions. Once the material is heated past the transition temperature, the materials crystalline phase melts causing the molecular chains to return to their original state [63].

Bodaghi et al. [4] show a 4D printing process where a stress is induced in the material during the fused deposition modelling printing process. The stress is unloaded when the material is submerged in warm water causing the material to deform into the desired configuration. This is a very simple, low cost method.

With a different approach, Zhang et al. [72] developed a biomimetic finger using azobenzene that undergoes trans-cis isomerization triggered by light. Irradiating certain parts of the finger would induce a local strain causing the finger to bend in the desired geometry, see Fig. 25. This photo-mechanical movement was reversed by heating the finger to re-configure it into the original shape. The reversibility and the range of motion in the paper have potential for many applications, but require the material to operate between 65°C and 100°C. The object also needs to be irradiated from specific direction to shape-shift into the required geometry, which might not be possible in certain applications.

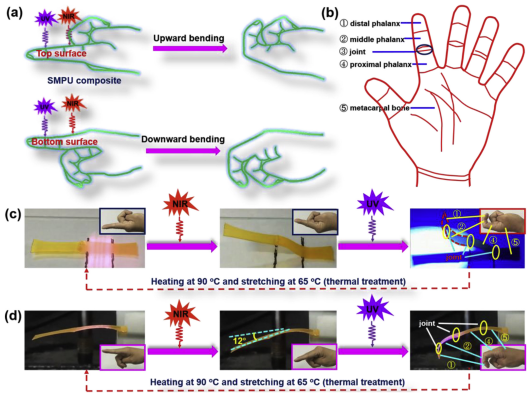

Fig. 25. Biomimetic finger, retrieved from [72]

G. Piezoelectric

Piezoelectric materials can be categorized into ceramics, polymers and composites. The mechanism behind the phenomenon is the piezoelectric effect, where a strain imposed on the material's crystal causes an electrical potential and vice versa [24]. The main advantage of piezoelectrics is the ability to accurately control their deformations since the electric potential, which can easily be controlled, is directly responsible for the induced strain. Below, we elaborate on the different categories. The differences, are summarized in Table I. We also provide some practical implementation in Fig. 26 and 27.

1) Ceramics: Piezoceramics are the most common piezoelectric materials as they are easy to manufacture at low cost. PZT is a well-known, stable example. These ceramics are easy to actuate and can operate at a high bandwith. However, their deformation is relatively small (≈0.1%) and the material is very brittle. To counteract the small deformations, the piezoceramics can be integrated in compliant mechanisms that amplify their motion [36]. Recently, Saravana Jothi and Hunt [35] have embedded a piezostack actuator and a rhombus motion amplifier in a hexagonal lattice to achieve in plane, controllable deformations, see Fig. 26.

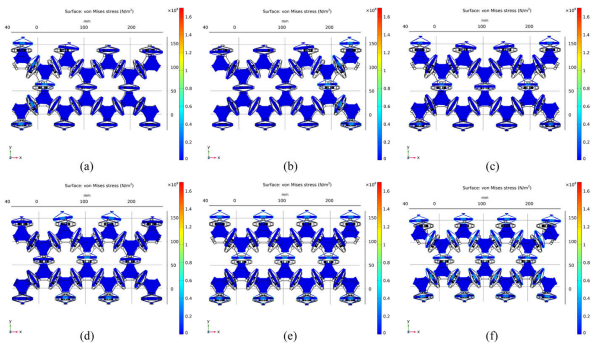

Fig. 26. The lattice deformation from embedded piezoelectrics, retrieved from [35]

2) Polymers: In bulk piezoelectric polymers the piezoelectric effect is caused by the molecular structure and orientation of the polymer [52]. Piezoelectric polymers are more flexible than their ceramic counterparts, but have a lower piezoelectric coefficient. They are mainly used in biomedical applications and electric fabrics. The most common piezoelectric polymer, polyvinylidene fluoride, is for example used in flexible, cm-scale bending actuators [55].

3) Composites: Piezoelectric composites are composed of piezoelectric ceramics and polymers. Their main benefit is that they possess a large piezoelectric constant, like piezoceremacis, while remaining flexible, like piezopolymers. The composites are suitable for integration in biomedical applications and can for example simulate muscle-like behaviour [45].

Habib et al. [24] provided an overview comparing the different piezoelectrics, see Table I.

TABLE I
A COMPARISON BETWEEN THE PIEZOELECTRICS RETRIEVED FROM [24]

Property or Metric	Ceramics	Polymers	Composites
Piezoelectric Constant	High	Low	High
Voltage Constant	Low	High	High
Flexibility	Low	High	Average
Electromechanical Coupling Factor	Average	Low	High
Curie Temperature	High	Low	Subjective[a]
Mechanical Quality Factor	Med	Low	High
Acoustic Impedance	High	Low	High
Chemical Reactivity	Low	Subjective[b]	Subjective[b]
Ease of Manufacturing	High	High	Low
Cost	High	Low	Subjective[a]
Density	High	Low	Average

[a] Depends on constituents and the manufacturing process.
[b] Depends on chemical composition and the presence of reactive functional groups.

Zhu et al. [74], used piezoelectric bending actuators to create a walking, steerable robot shown in Fig. 27. The researchers used a set of PZT wafers that were adhered to the top surface of an elastic substrate (the legs and body). By actuating the wafers, the front and hind legs could create a walking motion to locomote the robot forward with a speed of 330 mm/s (10 body-lengths per second). This was achieved by having 8600 stepping cycles per second.

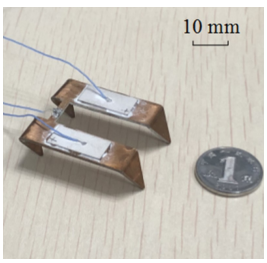

Fig. 27. Piezoelectric walker, retrieved from [74]

IV. Modelling and design

In this section, we review the existing modelling and design approaches for the previously described compliant bending mechanisms and smart material actuators. Most mechanisms from Sec. II, use small strains distributed over a large volume to create large net deformations. These compliant mechanisms often shown nonlinear geometric deformations. Thus, the modelling and design of these mechanisms difficult. Simple models do not suffice to guide the design and trial and error approaches require many iterations to succeed. Therefore, we look at systematic design approaches. Topology optimization (TO) is a design tool which is suitable for working with large nonlinear geometric deformations. TO is preferred to size or shape optimization as we do not need to presume an initial structural configuration. Using TO, we can maximize the net deformation while minimizing the material used. For the modelling, we focus on the utilisation of finite element methods (FEM). FEM is suitable to model the interaction between the smart materials and their stimuli to predict the behaviour of the material. Section IV-A reviews the modelling and design methods for the mechanisms found in Sec. II. Section IV-B studies the modelling and design approaches for the most common stimuli in smart material actuators from Sec. III; thermal and electric.

A. Modelling and design of compliant bending mechanisms

1) Uni-and bimorph bending: In this subsection we first review two analytical approaches to model uni-and bimorph bending mechanisms. Subsequently, we look into TO to enhance the the mechanisms by designing complex geometries instead of plane-symmetric layers.

Frecker and Aguilera [19] developed an analytical model for the unimorph bending of an electrostrictive polymer. A segment that uses an epoxy bonded active and passive polymer is considered. The analytical model determines the transverse stress in the active polymer from experimental data. To do so, the strain induced in the active material is measured under different applied electric fields. Subsequently, the data is fitted with a cubic polynomial to get an analytical expression of the transverse strain as a function of the applied electric field. After superimposing the calculated bending and extension forces, the curvature and extensional strain are found as a function of the design parameters and the curve-fitted experimental data. Guo et al. [23] study a similar laminated beam design where large deformations are induced by piezoelectric patches. The Absolute Nodal Coordinate Formulation (ANCF) is used to conveniently captures the nodal coordinates in the global coordinate system. The ANCF utilises slope vectors instead of rotation parameters such as Euler angles. The main benefit of this approach is that the slope vectors can be interpolated trough space and time similar to displacements [2].

Another modelling method is the material point method (MPM). The main benefit of MPM is that the problem is modelled with a set of material points or particles that are not connected by mesh elements. This prevents mesh distortion when a model is subjected to larger deformations, making MPM a suitable method for modelling soft bodies, soft robots or uni-and bimorph bending mechanisms that undergo large deformations [66]. Sato et al. [54] showed the potential of MPM by integrating a density filtering technique. This enabled the researchers to use MPM in TO. With several numerical experiments, locomoting walking and crawling robots are designed using this method. The method could be implemented for the optimization or design of uni or bimorph bending mechanisms that exhibit large pneumatic, magnetostrictive or photostrictive actuated deformations.

Yuhn et al. [71] studied the application of TO in morphable, self-actuating soft bodies. This allows uni-and bimorph mechanisms to be designed with complex geometries instead of plane-symmetric layers. They used a density-based approach that was modified to include time. Similar to [54], they use a MPM approach to model large deformations. First, the structure and movement are represented by a set of design variables. Subsequently, an objective function is defined to reflect the design's performance based on the dynamic task. During the gradient-based optimization, the method considers a spatial and a temporal design domain. The structure of the body and the layout of multiple actuators are optimized in the spatial domain while the temporal domain considers the time-varying actuation of the actuators. The method is developed and simulated for walking and climbing soft bodies. One of the simulations is a walking robot, see Fig. 28.

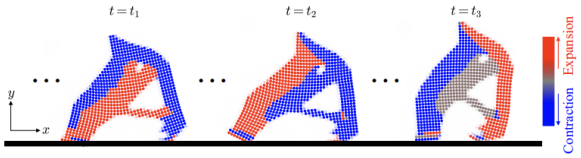

Fig. 28. Simulation of soft locomoting body, retrieved from [71]

2) Lamina emergent mechanisms: This subsection first reviews how existing studies show that LEMs can be modelled using FEM. Subsequently, we look into an analytical model, which gives insight in the design parameters of a LET joint. This analytical model, can be used to optimize the design of a LET joint.

The performance of the LET joints proposed by Jacobsen et al. [33] are studied and compared to their reinforced double laminated LET counterpart in [44]. Here, the researchers analyzed the joint with a FEM from the ABAQUS finite element software package using the NLGEOM function to account for nonlinear effects due to large displacements. The researchers report that the FEM has an error up to 3% compared to the theoretically calculated rotation induced by an applied bending moment. Similarly, Xie et al. [67] analyzed the ODLEJ joint in ANSYS Workbench, also FEM, which is capable of nonlinear and large deflection analysis. Here, an error up to 4% is found when comparing he theoretically calculated rotation with respect to the applied bending moment.

Bodappati et al. [5] proposed an analytical model to describe the bending and twisting behaviour of a layered piezo com-

posite, see Fig. 29. Twisting and bending are both common in LEMs. By altering the design parameters (length, width, thickness, fiber orientation and electric field magnitude) the bending or twisting can be designed. The twisting behaviour can possibly be used as an actuator by embedding the composite in the LET joints. The researchers suggest that the model can be adapted to be compatible with other stimuli-responsive materials.

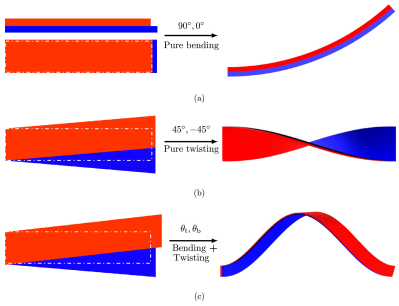

Fig. 29. Bending and twisting from bilayer piezocomposite, retrieved from [5]

3) O&K: As mentioned in Section II, there are several methodologies available that can systematically convert complex geometries into foldable polyhedrals [26] or design flat surfaces into rigid 3D meshes [43], see Fig. 5. To embed active elements in the O&K structures, Ge et al. [20] propose a theoretical model to provide guidelines for design parameters such as, fibre orientation, programming strains and temperature. Using their method, they created a self-folding and unfolding box and plane. Similarly, Yuan et al. [14, 70] studied the effect of fibre orientation and applied load to the programming of 3D-printable active components. More recently, Yuan et al. [69] provided a review for mechaniscs-based design strategies for 4D printing. This study provides a comprehensive overview of the existing design and manufacturing strategies for shape-shifting mechanisms. These manufacturing processes can even be accomplished with hobby 3D printers [46].

4) Wires: Palli et al. [49] developed a simple, inexpensive, small and lightweight TSA system, similar to a TSA system as shown in Fig. 12. They use an analytical approach to model the shortening of transmission system as a result of wires twisting together. The torque load on the motor is converted into a tension force on the wires, of which the elongation under the load can be determined. The study reports that the model is a useful tool to scale the design parameters of the mechanism, e.g., maximum stroke, velocity, force and dimensions. The researchers also propose an output feedback sliding manifold controller. This controller is based of [9] and similar to a high gain PID controller but offers a more robust control against disturbances.

B. Modelling and design of smart material actuators

This subsection covers modelling and design approaches of the most commonly found smart material stimuli found in Sec. III. First, we cover the thermal stimuli. Subsequently, we review electrical stimuli.

1) Thermal stimuli: Geiss et al. [21] proposed a design methodology for materials that undergo large deformations under stimulation by heat. Their methodology covers 4D printed, multilayer active materials. The methodology aims to design mechanisms with shape changing properties, that can be constructed with additive manufacturing methods. The method uses a LS approach with the combination of the extended finite element method (XFEM) and density-based TO to optimize the design. XFEM ensures that the clear boundary between material and void domains, which is obtained by the LS method, is retained during the optimization process with a fixed background mesh. As a result, the optimized design is better suited for additive manufacturing techniques. Within the material domains, the method uses a standard solid isotropic material penalization method to distinguish between the active and passive subdomains. The model was verified with several manufactured examples. It was shown that the method accurately predicted the design's behaviour in the physical experiments. It was also shown that the method successfully optimized a mechanism for maximum target displacement under a volume and end-stiffness constraint.

Kang et al. [38] proposed a framework that uses TO to design SMA actuated mechanisms. The framework assumes non-uniform temperature distributions. Thus, the framework can accurately capture the coupling between the phase transformation process and the evolution of the local temperature field. As a result, the TO is better equipped to optimize the two-way shape memory effect and the super elastic response of SMAs. With an experiment, the researchers show that the framework can successfully optimize the multi-material design of a SMA actuated gripper using an active SMA, an inactive material (BC) and with no material (void), see Fig. 30.

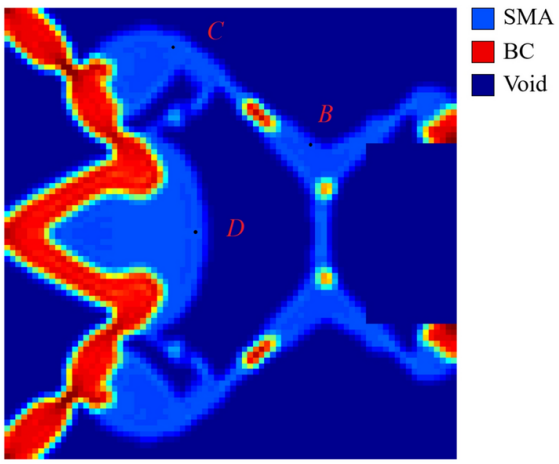

Fig. 30. Topology optimized SMA gripper, retrieved from [38]

Crews and Buckner [12] used a different approach to optimize and validate the design a robotic catheter. COMSOL (FEM) is used to describe the behaviour and to find the stresses in the SMA. The researchers used a free energy model to model the SMA phase transitions which subsequently predicted the thermo-mechanical compression and tension forces on the SMA. This stress is used in an analytical expression that finds the radius of curvature of the device. Subsequently, MATLAB uses a genetic algorithm (GA) to optimize the design. A GA is based on natural selection. The algorithm takes locally optimized solutions and crosses them with other solutions. The *children* of these solutions converge to a global optimum. Here, the objective is to minimize the radius of curvature within the boundaries of the design parameters such as SMA wire radius, catheter radius and Young's modulus of the flexible body. The researchers experimentally tested the catheter to verify their models. Here, stress-strain curves show that their model predict the major transition points and hysteresis of the system. It is also reported that the model predict the deformations more accurately at higher actuation temperatures.

2) Electric stimuli: Piezoelectric actuators often have very small deformations around 0.1% of their original size. To effectively use piezoelectrics in mechanisms where larger deformations are required, they can be combined with motion amplifiers. Several compliant amplifiers such as rhombus, Scott-Russel and bridge type, already exist [27, 31]. The existing amplifiers can achieve amplification up to several hundred times their input and are extensively researched. In addition to using existing motion amplifiers, one could use TO to achieve the desired deformation. Wang et al. [65] proposed a method to optimize the topology of the host structure and the position of movable PZT actuators simultaneously, see Fig. 31. The method used the level set (LS) model [13] to track the movements of the fixed size PZT actuators and a point-wise density field method [37] to optimize for the host structure. The proposed method is restricted to in-plane motion. Fang et al. [15] showed that the output of such volume constrained mechanisms does not only depend on the piezoelectric material distribution, but also on the polarization direction. They use the movable morphable void (MMV) method to remove piezoelectric material, leaving only the *required* material. The method uses a two-phase MMV where the first phase determines the distribution of the piezoelectric material and the second phase distinguishes between positive and negative polarization.

Tajeddini and Muliana [60] worked on the modelling of bi-morph bending induced by piezoelectric patches that are capable of larger deformations. They study a cantilever beam with several patches of piezoelectric material adhered to the top and bottom of the beam. The researchers adapted Reissner's finite deformation beam theory [53] to formulate the large deformations. The study shows that for large deformation, the nonlinear electro-mechanical response significantly differs from the linear response. It is also shown that time becomes an important factor to account for the relaxation behaviour of viscoelastic beams. The results are however not verified with experiments.

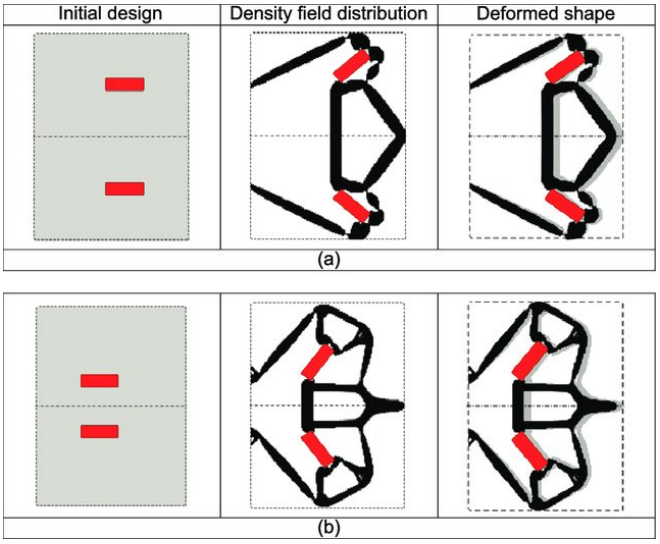

Fig. 31. TO with movable actuators, retrieved from [65]

V. Discussion

In this section, we first discuss the mechanisms that were found in Sec. II. Subsection V-A compares the different mechanisms, considers their advantages and drawbacks and looks into their possible use-cases. From this comparison, we select the mechanism that is most suitable for a smart actuated, controllable, compliant joint. Subsequently, we consider which smart material actuators from Sec. III best fit this application. Subsection V-B compares the different smart material actuators. We consider the response time, maximum deformation and controllability to select the most promising smart actuators. Finally, we discuss the modelling and design methods described in Sec. IV. Subsection V-C covers the use of FEM to model the chosen smart material actuator and how TO can optimize the mechanism.

A. Discussing compliant bending mechanisms

To assess and compare the out-of-plane bending or hinging behaviour of the mechanisms from Sec. II, we consider four criteria. First, we consider the sharpness of the out-of-plane bending angle. Mechanisms such as O&K, use *sharp bends* to fold into the desired direction whereas other mechanisms, like uni-and bimorph, have a *duller* curve to bend into the desired direction. Secondly, the stability can be an important factor. For a hinge-like application it is important that the mechanism can remain in the chosen position. Mechanisms like O&K, can only be fixed in certain stable positions such as their flat and fully deployed state. Thirdly, we aim to embed active materials within the mechanism for which not all mechanisms are suited. Finally, the compactness is to be considered. A comparative overview of the different mechanisms is presented in Table II.

TABLE II
Comparison of bending principles

	Uni-and bimorph	LEM	O&K	Wires
Sharp bends	+/-	+	++	++
Stability	++	++	-	++
Embedding actuation	++	++	+/-	+/-
Compactness	++	++	++	–

From the overview we can find that O&K and wires are the superior option when large, sharp bending angles are required. However, they come with some disadvantages. For the wired mechanisms, it is difficult to scale the mechanisms down. Previous research has shown that the wires suffer from friction, which can be critical on small scales. Additionally, the wires need to be pulled or twisted by some actuation unit which is difficult to scale down and embed within the mechanism.

As a result, wired mechanisms are most suited for hand-size grippers, where the frictional forces associated with the mechanism do not cause significant problems. Literature shows that wired mechanism are already successfully implemented in hand-size grippers [40]. These mechanisms can still be scaled down and their control can be improved. However, this is not the aim of this study.

O&K mechanisms are more suitable for smaller systems than wired mechanisms. They are able to create sharp folds with embedded active materials on small scales. However, these mechanisms are often moving between stable positions, e.g., from their unfolded flat state to their folded, deployed state and vice versa. This is a problem for a mechanism that needs to be positioned anywhere within its range of motion. However, these mechanisms are very promising when the system is desired to switch between two states. For example, they might be used to compactly house a sensor or part that can be folded out when needed. They offer an elegant solution for this type of housing/deployment application. However, it is difficult to make such a mechanisms versatile for use in multiple applications. These mechanisms can only deploy to the specific positions they are designed for and do not allow continuous change in their configuration. Additionally, O&K mechanisms are challenging mechanisms to embed with active elements. Their structure requires thin and sharp folding actuators, which are very difficult to realise.

O&K tessellations are not capable of large out-of-plane deformations. However, they are often arranged in a lattice like configuration where small deformations in the unit cells result in a large deformation over the whole system. This makes them an interesting candidate for morphing a surface into different curvatures. Literature shows theoretical research in this application [68] but there are no practical actuated experiments. This opens interesting studies in the development of these actuated, surface morphing tessellations. However, the number of applications for this mechanisms are limited. Shape-morphing a flat surface into a 3D curved surface, often requires stretching or folding of the flat sheet. Thus, many surface shapes will be difficult to realise.

Uni-and birmorph and LEMs are not able to create bends as sharp as the other mechanisms. However, they are better suited to be scaled down than wired mechanisms and they allow continuous change in configuration, unlike O&K mechanisms. Uni-and bimorph mechanisms and LEMs are naturally compliant and planar. This makes them suitable for planar manufacturing processes which is convenient to produce them at smaller scales and embed smart material actuators within the mechanism. Thus, uni-and bimorph mechanisms and LEMs are most fitting for compact, out-of-plane bending hinges. These actuated mechanism can be used in for example small scale robotics. The hinges or joints can be used to locomote the robot, or actuate compliant grippers by deforming the structure of the joint. This can significantly decrease the size of the robots, as we do not need mechanical actuators to control these elements. Literature shows uni-and bimorph mechanisms are already applied in these active hinges [18, 64] using SMA actuators. To the best knowledge of the author, actuated LET joints are not yet investigated in literature.

A bimorph mechanism and part of a LET joint are shown in Fig. 32. For the largest possible bending angle in a bimorph mechanism, the relative strain difference between the layers needs to be as large as possible. This can for example be done by contracting the blue layer and elongating the red layer. This means the mechanism will curve around a point in the e_1 and e_2 plane. The exact location of this point is not fixed, but a

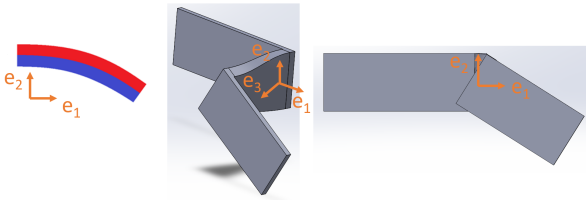

Fig. 32. Actuated bimorph mechanism and LET joint

function of the amount of elongation/contraction in the layers. This can impose difficulties in the control of the mechanism compared to the LET joint. The elongation/contraction in the LET joint induces twisting that shortens part of the mechanism. As a result, the point of rotation translates only over the e_3 vector. This is convenient, as the out-of-plane bending motion (in the e_1 and e_2 plane) will always be a rotation around the same point. Thus, for an active controllable hinge, an actuated LET joint might be more stable and easier to control than a bimorph mechanism.

B. Discussing smart material actuators

Actuating LET joints, will lead to an active hinge that can be used in for example small scale robotics. To find the most suitable form of actuation, we can consider the different smart material actuators presented in Sec. III. The discussed materials can be compared to each other, see Fig. 33. The overview presents the degree of deformation that can be achieved with each type of actuator. Here, a turning point is considered; sharp folds. Past this point, experiments show the actuator capability to completely fold in half with low radii of curvature, i.e., sharp bends. The response time shows the order of magnitude of the time required to reach maximum deformation. Note, the figure is not to scale. It is a comparative representation of the different actuation principles.

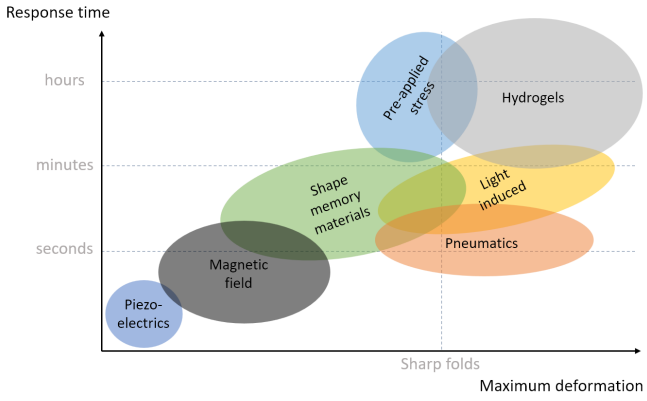

Fig. 33. An overview of the actuation principles and their respective bending angle and response time.

The overview clearly shows a trade-off between the shortest response time and the maximum deformation. It is most practical if the embedded actuators are activated by internal stimuli. This allows the user to locally control the mechanism without outside interference. Stimuli that have an area of effect, such as magnetic fields, are not desired. These stimuli, can influence a larger part of the mechanisms, which makes it difficult to accurately control deformations locally. For an active hinge, it is necessary that the actuation is reversible. The most feasible, internally stimulated, reversible actuators are SMM and piezoelectrics. These actuators are studied thoroughly and experimental data is available. The other actuators are either externally stimulated or non-reversible.

SMMs are already implemented in uni-and bimorph hinges. However, the bandwith of these actuators is limited to their heat dissipation which limits the actuation speed of a smart actuated hinge. Piezoelectrics can be actuated more accurately and faster, but their strains are smaller which limits the range of motion of the hinge. Theoretical research [5] shows that the twisting deformation in layered piezoelectric fibre composites generates large motion for small strains. This twisting deformation, is the bending principle in LET joints. Thus, the small induced strains in piezoelectrics might not limit range of motion of a LET hinge. Additionally, piezoelectrics provide large blocking forces and the hinges can be locked in position. Since this study was purely theoretical, experiments are needed. Piezoelectrics have a limited flexibility and it needs to be tested if they can comply with the required twisting motion. Boddapati et al. [5] also state that the large electric fields in their theoretical study are not usually feasible. To verify the feasibility of the piezoelectrics, a FEM can be done. This analysis needs analyze the maximum possible twisting deformation under influence of feasible electric fields.

C. Discussing modelling and design methods

Since we are looking to develop a controllable LET joint, embedded with a piezoelectric active element, we can use the analytical method proposed by Boddapati et al. [5]. This model provides an understanding of the geometry of the piezoelectric composite (PC), such as length, width, fibre orientation and polarization direction, and how it influences the behaviour of the PC. For a given design, the researchers report twisting capabilities of approximately 8.3 rotations per meter of PC, see Fig. 34.

However, the model assumes that the material is stimulated by infeasible, large electric fields. Thus, we expect that the actual achievable twisting is significantly lower. The model can be used as guidelines to develop a FEM, which analyzes the electro-mechanical induced deformations. With this FEM, we can model the amount of twisting that is possible for a PC when stimulated by feasible electric fields.

If the generated deformations are sufficiently large, we need to account for large non-linear geometric deformations. The FEM can be made with an available software package such as COMSOL, ABAQUS or ANSYS, as illustrated by [12, 44, 67] respectively. These package all have the ability to analyze large deformations.

To maximize the twisting in the PC, and thereby maximize the rotation in the joint, we can use density-based approach

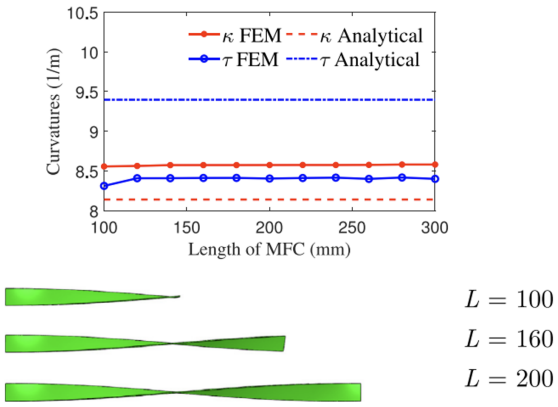

Fig. 34. Twisting behaviour of PC, retrieved from [5]

TO. Wang et al. [65] illustrated that TO can be used to optimize the shape of the host structure and location and orientation of fixed-size piezoelectric actuators. This however limits the design to using the fixed-size actuators. To optimize for actuators with non-predetermined geometries, a movable morphable components (MMC) method, similar to the MMV method from Fang et al. [15], can be considered. A two phase approach can be used to optimize the polarization direction of the actuators in addition to their geometry. The MMC piezoelectric actuators and their physical response to the stimulating electrical field can be modelled by the previously described FEM.

VI. Conclusion

Miniaturizing movable hinges or joints, can significantly increase the performance and sustainability of a mechanism. This miniaturization can be realized by embedding the actuation within the structure of the mechanism. Smaller parts have a lower mass and can be displaced with greater accuracy. Since the deformations are generated by changing the structure of the mechanism, we eliminate friction in moving parts. This lowers the required energy input making the mechanism more sustainable. Several engineering fields can benefit from the innovation in the development of these elements, such as robotics, minimally invasive surgery and high-tech industries. This study covers the different aspects that are to be considered when developing a smart actuated, compact, controllable, compliant joint. We divided this study into three parts covering the mechanism in Sec. II, the actuation in Sec. III and the modelling and design in Sec. IV.

We identified four mechanisms that can be used for compliant, out-of-plane deformations; uni-and bimorph, LEMs, O&K and wires. All mechanisms were compared in their ability to create sharp bends, their stability, their suitability to be embedded with smart material actuators and their compactness. Fitting applications are suggested for each mechanism and we theorized the most effective mechanisms for smart actuated compliant joints; the LET joint.

Furthermore, we describe the physical principles behind different smart material actuators. We compare the responsiveness of the different materials and find a clear trade-off between the bandwith and the maximum deformation in smart materials. After consideration, the most suitable materials for locally controlling the bending in an actuated compliant hinge are shape memory materials and piezoelectrics. Shape memory materials offer larger maximum deformation at the cost of slower response time as they are often limited by their heat dissipation. Piezoelectrics have smaller maximum deformation but are capable of a higher bandwith. Since piezoelectrics are capable of producing high blocking forces to lock an actuated joint in place, they are selected as the most promising smart actuated material.

Subsequently, we discuss how an analytical model of the twisting of a piezoelectric composite in a LET joint can be used to guide the development of a FEM model. This FEM model can conveniently describe the electro-mechanical response of the material when stimulated by an electric field. When needed, existing FEM software packages can also account for large, nonlinear geometric deformations, as illustrated by other studies. We also elaborate on the use of the FEM model in an density-based MMC TO approach to optimize the deformations in the design of the joint. This method enables the optimization of the size, shape and polarization direction of the active materials within their host-structure

Finally, we postulate a project proposal covering the required steps to model, design and test a smart actuated, compact, controllable, compliant joint.

References

[1] Tao Bai et al. “Zinc ion-triggered two-way macro-/microscopic shape changing and memory effects in high strength hydrogels with pre-programmed unilateral patterned surfaces”. In: *Soft Matter* 8 (25 2012), p. 6846. ISSN: 1744-683X. DOI: 10.1039/c2sm07364a.

[2] Peter Betsch, ed. *Structure-preserving Integrators in Nonlinear Structural Dynamics and Flexible Multibody Dynamics*. Vol. 565. Springer International Publishing, 2016, pp. 159–175. ISBN: 978-3-319-31877-6. DOI: 10.1007/978-3-319-31879-0.

[3] Priyanka Bhovad, Joshua Kaufmann, and Suyi Li. “Peristaltic locomotion without digital controllers: Exploiting multi-stability in origami to coordinate robotic motion”. In: *Extreme Mechanics Letters* 32 (Oct. 2019), p. 100552. ISSN: 23524316. DOI: 10.1016/j.eml.2019.100552.

[4] Mahdi Bodaghi et al. “4D Printing Self-Morphing Structures”. In: *Materials* 12 (8 Apr. 2019), p. 1353. ISSN: 1996-1944. DOI: 10.3390/ma12081353.

[5] Jagannadh Boddapati, Shaswat Mohanty, and Ratna Kumar Annabattula. “An analytical model for shape morphing through combined bending and twisting in piezo composites”. In: *Mechanics of Materials* 144 (May 2020), p. 103350. ISSN: 01676636. DOI: 10.1016/j.mechmat.2020.103350.

[6] David Bombara et al. “A Twisted String Actuator-Driven Soft Robotic Manipulator”. In: *IFAC-PapersOnLine* 54 (20 2021), pp. 141–146. ISSN: 24058963. DOI: 10.1016/j.ifacol.2021.11.166.

[7] Mustafa Boyvat, Je-Sung Koh, and Robert J. Wood. “Addressable wireless actuation for multijoint folding robots and devices”. In: *Science Robotics* 2 (8 July 2017). ISSN: 2470-9476. DOI: 10.1126/scirobotics.aan1544.

[8] Sebastien J.P. Callens and Amir A. Zadpoor. “From flat sheets to curved geometries: Origami and kirigami approaches”. In: *Materials Today* 21 (3 Apr. 2018), pp. 241–264. ISSN: 13697021. DOI: 10.1016/j.mattod.2017.10.004.

[9] A. Cavallo and C. Natale. “High-order sliding control of mechanical systems: theory and experiments”. In: *Control Engineering Practice* 12 (9 Sept. 2004), pp. 1139–1149. ISSN: 09670661. DOI: 10.1016/j.conengprac.2003.11.011.

[10] Chen Chen and Zhiguo Yi. “Photostrictive Effect: Characterization Techniques, Materials, and Applications”. In: *Advanced Functional Materials* 31 (22 May 2021), p. 2010706. ISSN: 1616-301X. DOI: 10.1002/adfm.202010706.

[11] Tian Chen et al. “Autonomous Deployment of a Solar Panel Using Elastic Origami and Distributed Shape-Memory-Polymer Actuators”. In: *Physical Review Applied* 11 (6 June 2019), p. 064069. ISSN: 2331-7019. DOI: 10.1103/PhysRevApplied.11.064069.

[12] John H Crews and Gregory D Buckner. “Design optimization of a shape memory alloy–actuated robotic catheter”. In: *Journal of Intelligent Material Systems and Structures* 23 (5 Mar. 2012), pp. 545–562. ISSN: 1045-389X. DOI: 10.1177/1045389X12436738.

[13] N. P. van Dijk et al. “Level-set methods for structural topology optimization: a review”. In: *Structural and Multidisciplinary Optimization* 48 (3 Sept. 2013), pp. 437–472. ISSN: 1615-147X. DOI: 10.1007/s00158-013-0912-y.

[14] Zhen Ding et al. “Direct 4D printing via active composite materials”. In: *Science Advances* 3 (4 Apr. 2017). ISSN: 2375-2548. DOI: 10.1126/sciadv.1602890.

[15] Lixue Fang et al. “Topology optimization of piezoelectric actuators using moving morphable void method”. In: *Structural and Multidisciplinary Optimization* 66 (2 Feb. 2023), p. 32. ISSN: 1615-147X. DOI: 10.1007/s00158-022-03469-6.

[16] E. Faran and D. Shilo. “Ferromagnetic Shape Memory Alloys—Challenges, Applications, and Experimental Characterization”. In: *Experimental Techniques* 40 (3 June 2016), pp. 1005–1031. ISSN: 0732-8818. DOI: 10.1007/s40799-016-0098-5.

[17] S. Felton et al. “A method for building self-folding machines”. In: *Science* 345 (6197 Aug. 2014), pp. 644–646. ISSN: 0036-8075. DOI: 10.1126/science.1252610.

[18] Amir Firouzeh et al. “Sensor and actuator integrated low-profile robotic origami”. In: IEEE, Nov. 2013, pp. 4937–4944. ISBN: 978-1-4673-6358-7. DOI: 10.1109/IROS.2013.6697069.

[19] Mary I Frecker and William M Aguilera. “Analytical modeling of a segmented unimorph actuator using electrostrictive P(VDF-TrFE) copolymer”. In: *Smart Materials and Structures* 13 (1 Feb. 2004), pp. 82–91. ISSN: 0964-1726. DOI: 10.1088/0964-1726/13/1/010.

[20] Qi Ge et al. “Active origami by 4D printing”. In: *Smart Materials and Structures* 23 (9 Sept. 2014), p. 094007. ISSN: 0964-1726. DOI: 10.1088/0964-1726/23/9/094007.

[21] Markus J. Geiss et al. “Combined Level-Set-XFEM-Density Topology Optimization of Four-Dimensional Printed Structures Undergoing Large Deformation”. In: *Journal of Mechanical Design* 141 (5 May 2019). ISSN: 1050-0472. DOI: 10.1115/1.4041945.

[22] Steven W. Grey, Fabrizio Scarpa, and Mark Schenk. “Embedded Actuation for Shape-Adaptive Origami”. In: *Journal of Mechanical Design* 143 (8 Aug. 2021). ISSN: 1050-0472. DOI: 10.1115/1.4049880.

[23] Xian Guo et al. “Large deformations of piezoelectric laminated beams based on the absolute nodal coordinate formulation”. In: *Composite Structures* 275 (Nov. 2021), p. 114426. ISSN: 02638223. DOI: 10.1016/j.compstruct.2021.114426.

[24] Mahpara Habib, Iza Lantgios, and Katherine Hornbostel. “A review of ceramic, polymer and composite piezoelectric materials”. In: *Journal of Physics D:*

Applied Physics 55 (42 Oct. 2022), p. 423002. ISSN: 0022-3727. DOI: 10.1088/1361-6463/ac8687.

[25] E. Hawkes et al. "Programmable matter by folding". In: *Proceedings of the National Academy of Sciences* 107 (28 July 2010), pp. 12441–12445. ISSN: 0027-8424. DOI: 10.1073/pnas.0914069107.

[26] E. A. Peraza Hernandez, D. J. Hartl, and D. C. Lagoudas. "Design and simulation of origami structures with smooth folds". In: *Proceedings of the Royal Society A: Mathematical, Physical and Engineering Sciences* 473 (2200 Apr. 2017), p. 20160716. ISSN: 1364-5021. DOI: 10.1098/rspa.2016.0716.

[27] Jaroslav Hricko and Štefan Havlík. *Compliant Mechanisms for Motion/Force Amplifiers for Robotics*. 2020, pp. 26–33. DOI: 10.1007/978-3-030-19648-6_4.

[28] W.M. Huang et al. "Shape memory materials". In: *Materials Today* 13 (7-8 July 2010), pp. 54–61. ISSN: 13697021. DOI: 10.1016/S1369-7021(10)70128-0.

[29] Agustin Iniguez-Rabago and Johannes T.B. Overvelde. "From rigid to amorphous folding behavior in origami-inspired metamaterials with bistable hinges". In: *Extreme Mechanics Letters* 56 (Oct. 2022), p. 101881. ISSN: 23524316. DOI: 10.1016/j.eml.2022.101881.

[30] Leonid Ionov. "Hydrogel-based actuators: possibilities and limitations". In: *Materials Today* 17 (10 Dec. 2014), pp. 494–503. ISSN: 13697021. DOI: 10.1016/j.mattod.2014.07.002.

[31] Sohail Iqbal and Afzaal Malik. "A review on MEMS based micro displacement amplification mechanisms". In: *Sensors and Actuators A: Physical* 300 (Dec. 2019), p. 111666. ISSN: 09244247. DOI: 10.1016/j.sna.2019.111666.

[32] Joseph O. Jacobsen et al. "Lamina Emergent Mechanisms and Their Basic Elements". In: *Journal of Mechanisms and Robotics* 2 (1 Feb. 2010). ISSN: 1942-4302. DOI: 10.1115/1.4000523.

[33] Joseph O. Jacobsen et al. "Lamina Emergent Torsional (LET) Joint". In: *Mechanism and Machine Theory* 44 (11 Nov. 2009), pp. 2098–2109. ISSN: 0094114X. DOI: 10.1016/j.mechmachtheory.2009.05.015.

[34] Kwang-Un Jeong et al. "Three-dimensional actuators transformed from the programmed two-dimensional structures via bending, twisting and folding mechanisms". In: *Journal of Materials Chemistry* 21 (19 2011), p. 6824. ISSN: 0959-9428. DOI: 10.1039/c0jm03631e.

[35] N. S. Saravana Jothi and A. Hunt. "Active mechanical metamaterial with embedded piezoelectric actuation". In: *APL Materials* 10 (9 Sept. 2022), p. 091117. ISSN: 2166-532X. DOI: 10.1063/5.0101420.

[36] Ho Je Jung and Jung Hyun Kim. "Novel piezo driven motion amplified stage". In: *International Journal of Precision Engineering and Manufacturing* 15 (10 Oct. 2014), pp. 2141–2147. ISSN: 2234-7593. DOI: 10.1007/s12541-014-0574-8.

[37] Zhan Kang and Yiqiang Wang. "Structural topology optimization based on non-local Shepard interpolation of density field". In: *Computer Methods in Applied Mechanics and Engineering* 200 (49-52 Dec. 2011), pp. 3515–3525. ISSN: 00457825. DOI: 10.1016/j.cma.2011.09.001.

[38] Ziliang Kang and Kai A. James. "Multiphysics design of programmable shape-memory alloy-based smart structures via topology optimization". In: *Structural and Multidisciplinary Optimization* 65 (1 Jan. 2022), p. 24. ISSN: 1615-147X. DOI: 10.1007/s00158-021-03101-z.

[39] Sajeewa D. Katugampala et al. "Design and Characterization of a Novel Vacuum Bending Actuator and a Bimorph: for Preliminary Use in a Continuum Robot Arm". In: IEEE, Nov. 2019, pp. 263–268. ISBN: 978-1-7281-3458-1. DOI: 10.1109/CIS-RAM47153.2019.9095543.

[40] Revanth Konda et al. "Anthropomorphic Twisted String-Actuated Soft Robotic Gripper With Tendon-Based Stiffening". In: *IEEE Transactions on Robotics* 39 (2 Apr. 2023), pp. 1178–1195. ISSN: 1552-3098. DOI: 10.1109/TRO.2022.3224774.

[41] B. Kundys. "Photostrictive materials". In: *Applied Physics Reviews* 2 (1 Mar. 2015), p. 011301. ISSN: 1931-9401. DOI: 10.1063/1.4905505.

[42] Ville Laitinen et al. "Giant 5.8% magnetic-field-induced strain in additive manufactured Ni-Mn-Ga magnetic shape memory alloy". In: *Scripta Materialia* 208 (Feb. 2022), p. 114324. ISSN: 13596462. DOI: 10.1016/j.scriptamat.2021.114324.

[43] Robert J. Lang and Larry Howell. "Rigidly Foldable Quadrilateral Meshes From Angle Arrays". In: *Journal of Mechanisms and Robotics* 10 (2 Apr. 2018). ISSN: 1942-4302. DOI: 10.1115/1.4038972.

[44] Buchuan Ma et al. "Design and Performance Analysis of Lamina Emergent Torsional Joints Based on Double-Laminated Material Structure". In: *Applied Sciences* 12 (5 Mar. 2022), p. 2642. ISSN: 2076-3417. DOI: 10.3390/app12052642.

[45] Aleksey V. Maksimkin et al. "Electroactive Polymer-Based Composites for Artificial Muscle-like Actuators: A Review". In: *Nanomaterials* 12 (13 July 2022), p. 2272. ISSN: 2079-4991. DOI: 10.3390/nano12132272.

[46] Teunis van Manen, Shahram Janbaz, and Amir A. Zadpoor. "Programming 2D/3D shape-shifting with hobbyist 3D printers". In: *Materials Horizons* 4 (6 2017), pp. 1064–1069. ISSN: 2051-6347. DOI: 10.1039/C7MH00269F.

[47] Robin M. Neville, Fabrizio Scarpa, and Alberto Pirrera. "Shape morphing Kirigami mechanical metamaterials". In: *Scientific Reports* 6 (1 Aug. 2016), p. 31067. ISSN: 2045-2322. DOI: 10.1038/srep31067.

[48] A.G. Olabi and A. Grunwald. "Design and application of magnetostrictive materials". In: *Materials Design* 29 (2 Jan. 2008), pp. 469–483. ISSN: 02613069. DOI: 10.1016/j.matdes.2006.12.016.

[49] Gianluca Palli et al. “Modeling and Control of the Twisted String Actuation System”. In: *IEEE/ASME Transactions on Mechatronics* 18 (2 Apr. 2013), pp. 664–673. ISSN: 1083-4435. DOI: 10.1109/TMECH.2011.2181855.

[50] Nuri Park and Jaeyun Kim. “Hydrogel-Based Artificial Muscles: Overview and Recent Progress”. In: *Advanced Intelligent Systems* 2 (4 Apr. 2020), p. 1900135. ISSN: 2640-4567. DOI: 10.1002/aisy.201900135.

[51] Nicholas A. Peppas and Allan S. Hoffman. *Hydrogels*. Elsevier, 2020, pp. 153–166. DOI: 10.1016/B978-0-12-816137-1.00014-3.

[52] Khaled S Ramadan, D Sameoto, and S Evoy. “A review of piezoelectric polymers as functional materials for electromechanical transducers”. In: *Smart Materials and Structures* 23 (3 Mar. 2014), p. 033001. ISSN: 0964-1726. DOI: 10.1088/0964-1726/23/3/033001.

[53] Eric Reissner. “On one-dimensional finite-strain beam theory: The plane problem”. In: *Zeitschrift für angewandte Mathematik und Physik ZAMP* 23 (5 Sept. 1972), pp. 795–804. ISSN: 0044-2275. DOI: 10.1007/BF01602645.

[54] Yuki Sato et al. “Topology optimization of locomoting soft bodies using material point method”. In: (Mar. 2022). DOI: 10.1007/s00158-023-03502-2. URL: http://arxiv.org/abs/2203.16793%20http://dx.doi.org/10.1007/s00158-023-03502-2.

[55] Sobhan Sharafkhani and Mehrdad Kokabi. “High performance flexible actuator: PVDF nanofibers incorporated with axially aligned carbon nanotubes”. In: *Composites Part B: Engineering* 222 (Oct. 2021), p. 109060. ISSN: 13598368. DOI: 10.1016/j.compositesb.2021.109060.

[56] Moshe Shoham. “Twisting Wire Actuator”. In: *Journal of Mechanical Design* 127 (3 May 2005), pp. 441–445. ISSN: 1050-0472. DOI: 10.1115/1.1866156.

[57] A Singh et al. “Extreme on-demand contactless modulation of elastic properties in magnetostrictive lattices”. In: *Smart Materials and Structures* 31 (12 Dec. 2022), p. 125005. ISSN: 0964-1726. DOI: 10.1088/1361-665X/ac9cac.

[58] David C. Stanier, Jacopo Ciambella, and Sameer S. Rahatekar. “Fabrication and characterisation of short fibre reinforced elastomer composites for bending and twisting magnetic actuation”. In: *Composites Part A: Applied Science and Manufacturing* 91 (Dec. 2016), pp. 168–176. ISSN: 1359835X. DOI: 10.1016/j.compositesa.2016.10.001.

[59] Subramanian Sundaram et al. “3D-Printed Self-Folding Electronics”. In: *ACS Applied Materials Interfaces* 9 (37 Sept. 2017), pp. 32290–32298. ISSN: 1944-8244. DOI: 10.1021/acsami.7b10443.

[60] Vahid Tajeddini and Anastasia Muliana. “Nonlinear deformations of piezoelectric composite beams”. In: *Composite Structures* 132 (Nov. 2015), pp. 1085–1093. ISSN: 02638223. DOI: 10.1016/j.compstruct.2015.06.041.

[61] N. Torras et al. “Bending kinetics of a photo-actuating nematic elastomer cantilever”. In: *Applied Physics Letters* 99 (25 Dec. 2011), p. 254102. ISSN: 0003-6951. DOI: 10.1063/1.3670502.

[62] Boran Wang et al. “Design, modelling and simulation of soft grippers using new bimorph pneumatic bending actuators”. In: *Cogent Engineering* 4 (1 Jan. 2017), p. 1285482. ISSN: 2331-1916. DOI: 10.1080/23311916.2017.1285482.

[63] Lu Wang et al. “Shape Memory Polymer Fibers: Materials, Structures, and Applications”. In: *Advanced Fiber Materials* 4 (1 Feb. 2022), pp. 5–23. ISSN: 2524-7921. DOI: 10.1007/s42765-021-00073-z.

[64] Wei Wang et al. “Soft composite hinge actuator and application to compliant robotic gripper”. In: *Composites Part B: Engineering* 98 (Aug. 2016), pp. 397–405. ISSN: 13598368. DOI: 10.1016/j.compositesb.2016.05.030.

[65] Yiqiang Wang et al. “Topological design of compliant smart structures with embedded movable actuators”. In: *Smart Materials and Structures* 23 (4 Apr. 2014), p. 045024. ISSN: 0964-1726. DOI: 10.1088/0964-1726/23/4/045024.

[66] Z. Wieckowski. “The material point method in large strain engineering problems”. In: *Computer Methods in Applied Mechanics and Engineering* 193 (39-41 Oct. 2004), pp. 4417–4438. ISSN: 00457825. DOI: 10.1016/j.cma.2004.01.035.

[67] Zhongtian Xie, Lifang Qiu, and Debin Yang. “Design and analysis of Outside-Deployed Lamina Emergent Joint (OD-LEJ)”. In: *Mechanism and Machine Theory* 114 (Aug. 2017), pp. 111–124. ISSN: 0094114X. DOI: 10.1016/j.mechmachtheory.2017.03.011.

[68] Ying Yu, Yan Chen, and Glaucio Paulino. “Programming curvatures by unfolding of the triangular Resch pattern”. In: *International Journal of Mechanical Sciences* 238 (Jan. 2023), p. 107861. ISSN: 00207403. DOI: 10.1016/j.ijmecsci.2022.107861.

[69] Chao Yuan, Tongqing Lu, and T.J. Wang. “Mechanics-based design strategies for 4D printing: A review”. In: *Forces in Mechanics* 7 (May 2022), p. 100081. ISSN: 26663597. DOI: 10.1016/j.finmec.2022.100081.

[70] Chao Yuan et al. “3D printed active origami with complicated folding patterns”. In: *International Journal of Precision Engineering and Manufacturing-Green Technology* 4 (3 July 2017), pp. 281–289. ISSN: 2288-6206. DOI: 10.1007/s40684-017-0034-x.

[71] Changyoung Yuhn et al. “4D topology optimization: Integrated optimization of the structure and movement of self-actuating soft bodies”. In: (Feb. 2023). URL: http://arxiv.org/abs/2302.00905.

[72] Peng Zhang et al. “UV–vis–NIR light-induced bending of shape-memory polyurethane composites doped with azobenzene and upconversion nanoparticles”. In: *Poly-*

mer 178 (Sept. 2019), p. 121644. ISSN: 00323861. DOI: 10.1016/j.polymer.2019.121644.

[73] Zeang Zhao et al. "Origami by frontal photopolymerization". In: *Science Advances* 3 (4 Apr. 2017). ISSN: 2375-2548. DOI: 10.1126/sciadv.1602326.

[74] Pancheng Zhu et al. "A steerable miniature legged robot based on piezoelectric bending actuators". In: *Smart Materials and Structures* 29 (4 Apr. 2020), p. 045009. ISSN: 0964-1726. DOI: 10.1088/1361-665X/ab74bb.

3 Designing, manufacturing and testing bimorph piezoelectric twisting actuators

Main paper

Designing, manufacturing and testing bimorph piezoelectric twisting actuators

Baaij, T. A.
Department of Precision and Microsystems Engineering
Delft University of Technology
Delft, Netherlands
t.a.baaij@student.tudelft.nl

Abstract*—Smart material actuators rely on the deformation of bulk material to achieve their desired deformation or motion. By doing so, they eliminate the need for traditional moving components such as hinges. Embedding smart materials in mechanisms can greatly reduce the size and energy required to operate systems which makes it more efficient and sustainable. As a result, smart material actuators have applications in small scale robotics, high-tech systems and shape morphing mechanisms. Research on smart material actuators shows many approaches to achieve elongating, contracting or bending deformation. However, little to no research is conducted on smart material actuators capable of manipulating rotation. Smart material twisting actuators enable control over an additional degree of freedom in compact shape-morphing mechanisms which is not possible with other smart material actuators. This study develops a planer actuator that generates out-of-plane rotation. It first investigates different out-of-plane deformation modes and how they can be used to achieve the desired motion. Based on an analytical model on the shape morphing of piezoelectric macro fibre composites, a methodology is developed to generate out-of-plane twisting deformation. This concept is used to design a carbon black electrode pattern, which can be spray-deposited on a kapton substrate. This electrode is subsequently used to selectively actuate parts of a P(VDF-TrFE- CTFE) polymer layer. The selective stimulation of the layer results in the desired twisting deformation. This study demonstrates how flat designs can be laminated in a planar additive manufacturing process to induce complex 3D motion. The spray-deposition process was capable of manufacturing bimorph actuators with a 1.6mm resolution. The resulting actuators have a length of 40.73mm and a width of 10.20 to 20.38mm and a thickness of 120 to 139μm. The experiments are used to characterize the effect of the design parameters such as actuator width and thickness on the magnitude of the deformation. As theorized in the analytical model, the thinner more slender samples show the largest rotation which is measured to rotate up to 3.38 degrees. From the experiments it is also found that thinner samples show dielectric breakdown at much lower voltages, around 100V, compared to thicker samples from the same design that performed up to 480V. The study also investigates the quality of the deformation of the actuators, i.e. pure twisting or a combination of twisting and bending deformation. It is verified that uneven layers or asymmetric actuators show significant unimorph bending behaviour, with displacements up to 1.5mm while rotating 3.38 degrees. To the author's best knowledge, this study presents the first working prototypes of fast-response smart material twisting actuators.

I. Introduction

Scaling down mechanisms can improve their performance and lower their power consumption. Smaller parts have a lower mass which can result in faster and more efficient operation with a lower energy input. Thus, miniaturized mechanisms are more sustainable with better performance. Miniaturisation can be applied to advance many engineering fields such as robotics, minimally invasive surgery or high-tech industries.

To meet the increasing innovation is these fields, researchers are devoting significant effort to study and develop smart material actuators. Smart material actuators can convert energy from one physical domain to another. For example, thermal energy can be used to impose a strain on a material, thus converting thermal energy to mechanical energy. Embedding smart materials in mechanisms can greatly reduce the size and energy required to operate the system which makes it more efficient and sustainable. Smart materials can be embedded in planar structures by the means of planar manufacturing processes and additive manufacturing. By deforming bulk material within the mechanism, moving components which cause friction, such as hinges, can be eliminated.

In literature, several smart materials are identified. These smart materials can be actuated by external stimuli such as light [11], magnetic fields [13, 14] and heat [3, 5, 16]. It is found that smart material actuator generally show a trade-off between the magnitude of the deformation and the actuation speed. Most experimental studies show examples of elongating, contracting or bending smart material actuators. Only recently, researchers started exploring smart material actuators that manipulate a more complex deformation mode; rotation. Lee et al. [10] published a study on a shape memory alloy twisting actuator. These actuators approached +57° and -45.7° after 6.4s which increased to +120.3° and -97° after 102.4s. This actuator shows large rotations but the actuation speed is limited by the heat dissipation of the system. With the current technology, the actuation speed and responsiveness of smart mechanisms that require rotation is severely limited. To the author's best knowledge, fast response smart material twisting actuators are not yet experimentally studied. One category of smart materials that has a fast response, is piezoelectric materials [4]. Therefore, this study develops a novel piezoelectric, fast response twisting actuator.

First, this study explores different out-of-plane deformation modes in Subsec. II-A. An analytical model for the defor-

mation in a bilayer macro fibre composite by Boddapati et al. [1] is used. This model describes how the direction of piezoelectric macro fibres determines the out-of-plane deformation mode of the composite. Boddapati et al. report that pure twisting deformation can be achieved with fibres in a $\theta_t = +45°$ and $\theta_b = -45°$ direction, see Fig. 2. Subsequently, we theorize how a layered structure can mimic the behaviour of the piezoelectric macro fibres. This leads to a conceptual design that has thin diagonal features that can actuate thin diagonal lines across an electroactive layer. By stacking this design, stimulation can be achieved along the $\theta_t = +45°$ and $\theta_b = -45°$ direction. The design parameters of the conceptual design are compared to the analytical model. It is found that the actuator is expected to produce maximum twisting deformation for thin, slender electrode designs.

In Subsec. II-B we discuss how an existing spray deposition machine can be modified to manufacture the design. By modifying the hard-and software, several electrode patterns and electroactive layers can be spray-deposited to manufacture the bimorph structure. A laser surface treatment is implemented to improve the adhesion of the materials to the substrate. The full manufacturing process with all printing parameters is presented and an an experimental setup is created to measure the rotation for the manufactured samples.

In Sec. III four different electrode designs are generated and manufactured using the methodology from Sec. II. These actuators are examined using a scanning electron microscope and their performance is compared to the cross-sections of the actuators. The samples are experimentally tested and the results are evaluated. Finally, recommendations for future work are proposed in Sec. V.

II. Methodology

This section describes the design methodology for the development of a bimorph piezoelectric twisting actuator. First, Subsec. II-A provides a theoretical model by Boddapati et al. [1]. From this model, a design concept is developed that generates twisting motion from a planar bimorph structure. Subsequently, Subsec. II-B discusses a recently developed spray-deposition device [7] and how it can be used to manufacture the design. Here, we discuss the current state of the machine and what materials it uses. The required upgrades to realise the design are provided and the manufacturing process is described. Finally, in Subsec. II-C an experimental setup is developed that can measures the twisting of the actuators using two lasers.

A. Design concept and modelling

1) Theory: The out-of-plane bending motion of planar mechanisms can be categorised in two distinct modes, bending and twisting and a combination of the two. These deformation modes are shown in Fig. 1. Here, the initially flat red and blue plane are the manufacturing plane. Despite their planar structure, these mechanisms can provide out-of-plane motion.

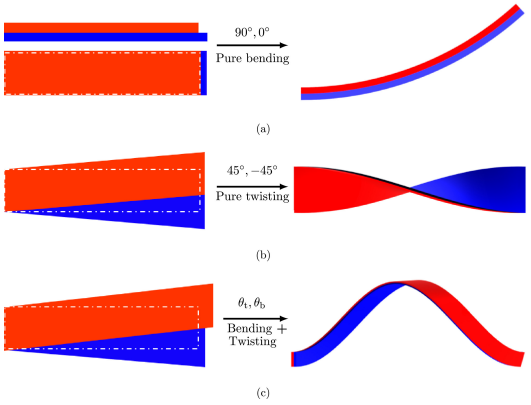

Fig. 1: Out-of-plane deformations of planar structures, retrieved from [1]

Boddapati et al. [1], propose an analytical model for the shape morphing of piezoelectric composites into these modes. They model a bilayer composite containing piezo macro fibres, see Fig. 2. The relative orientation of these fibres in the top and bottom layer, θ_t and θ_b respectively, determines the deformation mode of the composite when actuated. In this model, the fibres are actuated by applying an electrical field along the fibre direction. The authors report that pure twisting deformation along the length direction is achieved when the piezo macro fibres are aligned along $\theta_t = +45°$ and $\theta_b = -45°$.

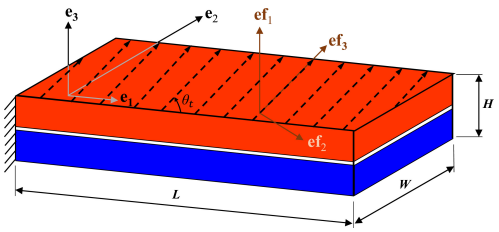

Fig. 2: Bilayer macro fibre composite setup, retrieved from [1]

By applying an electric potential on the electrodes, an electric field, E, is generated along the thickness direction of the electroactive material (EAM). This generates a strain along the direction of E (d_{33}) and perpendicular to E (d_{31}), see Fig. 3. By depositing thin lines of electrodes, the most prominent deformation will occur in the direction of said lines. These lines can be compared to the piezoelectric macro fibres from the analytical model and a similar behaviour is expected. The electrodes that actuate these thin EAM fibres can be laminated into a structure that independently actuates parts of the EAM in a $\theta_t = +45°$ and $\theta_b = -45°$ direction, to achieve twisting behaviour.

2) Conceptual design: From theory we concluded that thin lines of electrodes in a $\theta_t = +45°$ and $\theta_b = -45°$ direction can induce twisting. These thin lines of electrodes can stim-

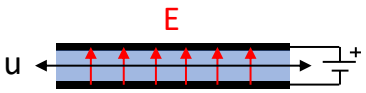

Fig. 3: Spray deposited actuator behaviour

ulate an EAM and generate strains along the electrodes. By layering the electrodes, a moment is created around a neutral axis. All these lines need to be supplied with a voltage to create the required electric field to stimulate the EAM. To do so, a *central voltage hub* needs to connect all the lines. This is hub is placed in the center of the electrode to distribute the conductive material as symmetric as possible. At the edge of the design, the voltage potential needs to be applied at a *voltage terminal* to stimulate the EAM. The resulting design is shown in Fig. 4.

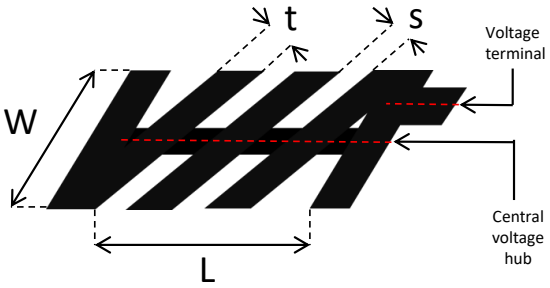

Fig. 4: Electrode design parameters

These thin electrode lines can be characterized by the thickness of the lines (t), the spacing between the lines (s), the width of the electrode (W) and the length of the electrode (L). This design concept can be stacked to achieve the desired $\theta_t = +45°$ and $\theta_b = -45°$ actuation direction with a laminated bimorph actuator, see Fig. 5.

To prevent a shorted circuit, the top and bottom electrodes need to be separated by a dielectric EAM. This can be realised by depositing a relatively thick layer of EAM compared to the electrodes. This also delays the dielectric breakdown of the piezoelectric material when increasing the applied voltage. The $+45°$ and $-45°$ patterns are stacked on the top and bottom of a kapton substrate which acts as a neutral axis. Kapton is an excellent insulator which ensures that there is no connection between the top and bottom half of the actuator.

3) Analytical model of twisting performance: From [1], an approximation of the twisting per meter, τ, can be found for piezoelectric macro fibre composites, see Eq. 1. Here, E is the electric field stimulating the actuator in the direction of the fibres, e_{33} and e_{31} are elements of the piezoelectric stress tensor, C_{11} and C_{12} are elements of the elastic stiffness tensor

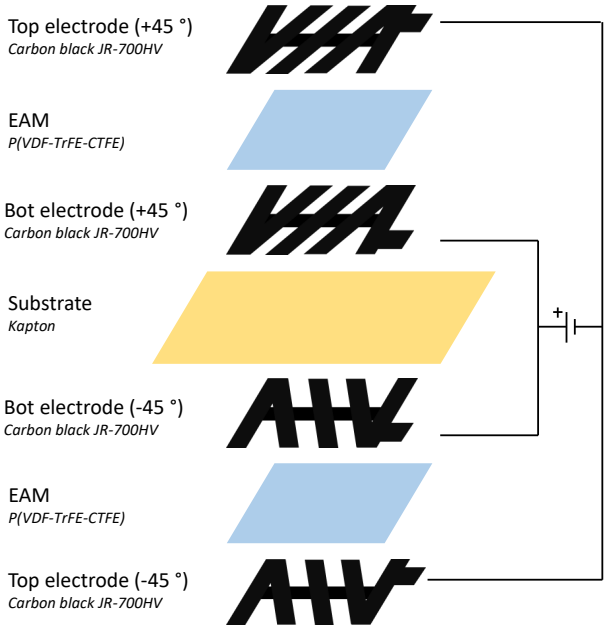

Fig. 5: Actuator layout

and H is the thickness of the actuator where the indices are shown in Fig. 2. In Eq. 1, the design parameters are isolated in the second term of the equation.

$$\tau \approx \frac{3E\left(e_{33}-e_{31}\right)}{C_{11}-C_{12}} \frac{1}{2.65H+0.017W+0.057\frac{W^2}{100H}} \quad (1)$$

The theoretical model is based on the composite being a thin slender beam, where $L \geq 10W$ and $W \geq 10H$. To compare the electrode lines to closely packed, thin piezoelectric macro fibres, design parameters t and s need to be as small as possible. To evaluate the effect of the design parameters, the first fraction of Eq. 1 is prescribed to be constant. Thus we see $\tau\left(H, W^2\right)$. Since the magnitude of the rotation is dependent on W^2 and the width can easily be changed in the electrode design, W is considered the most influential design parameter. With the half the model unknown, we can only qualitatively asses the influence of W, which is shown in Fig. 6.

Here, it is shown that τ decreases exponentially with respect to W when H is kept constant at $100\mu m$. H is the thickness of the actuator and thus a summation of the thickness of all the layers of the design. As mentioned previously, the EAM needs to be as thick as possible to prevent dielectric breakdown at higher voltages.

B. Printer setup and manufacturing process

In this subsection, we describe the manufacturing process. The spray-deposition machine that was used to manufacture the actuators is shown in Fig. 7.

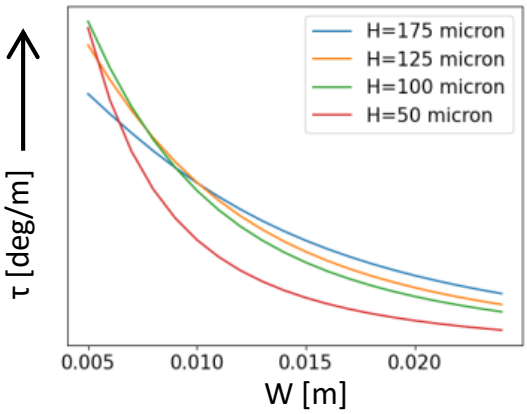

Fig. 6: Characterization of the twisting performance with respect to the design parameters

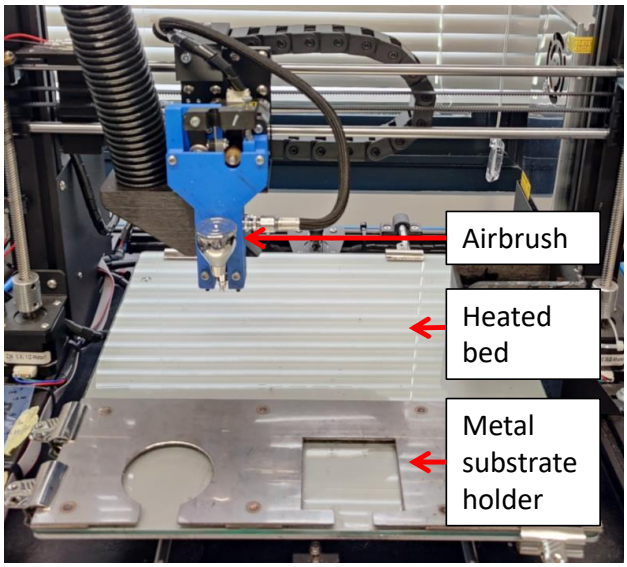

Fig. 7: Spray-deposition printer

1) Spray deposition machine: A 3D printer that is modified for automated spray-deposition [7] is used to manufacture the actuators. This device can deposit electric conductive carbon ink, JR-700HV, and an electroactive polymer (EAP), P(VDF-TrFE-CTFE) polymer in user specified designs. This machine utilises an airbrush to deposit layers of each material with a printing resolution of $\approx$ 0.5mm. Thus, the machine can deposit all layers in the required design as shown in Fig. 5.

A specialized metal printbed adapter is developed to attach the samples. This adapter ensures alignment and allows heating during printing. To generate the code that controls the printer, we modified an open source design program; Inkscape. In this program, the user can draw a design which is converted in the g-code that controls the printer.

2) Actuator manufacturing: The electrode patterns are from a carbon based conductive ink, JR-700HV and the EAM is a P(VDF-TrFE-CTFE) solution. The layers are spray-deposited on kapton film, see Fig. 5.

With the metal substrate aligner, we can heat the samples during the manufacturing process. The heating function allows for solvents in the EAP solution to evaporate more quickly during the printing. As a result, the EAP solution can be synthesized using higher concentration of solvents which prevents clogging in the airbrush. The EAP solution that is used for the manufacturing of the actuators is a 5wgt% P(VDF-TrFE-CTFE) in a 1:9 dimethyl sulfoxide (DMSO) to methylethylketon (MEK) solution.

The electrode design is printed on a kapton substrate due to its excellent electrical properties. The kapton substrate has a thickness of 50μm, thus is very flexible. Additionally, kapton has very good thermal properties which is necessary to anneal the EAP at 110° [15]. However, kapton has a smooth, semi-hydrophobic surface and liquid droplets are easily removed. As a result, the spray-deposited carbon ink forms pools on the material. When depositing ink, the air pressure will push these pools over the substrate, placing the conductive liquid in undesired locations on the substrate. To prevent pools from forming, the electrodes are deposited in several thin layers where each layer deposits a small amount of ink that can dry quickly. The kapton substrate needs treatment to ensure proper adhesion of the first layer of spray deposited electrode. This study considered two possible surface treatment methods; plasma treatment and laser treatment.

3) Surface treatment: To improve the wettability of kapton, small spots can be etched into the surface with a laser [6, 12]. Using a *Lasea* laser the kapton is treated. Experiments show good adhesion for a spot diameter of 20μm with 50μm spacing. However, varying the spot size and spacing did not result in significant differences. Since the manufacturing of the actuators is a proof of concept, this is not further investigated. The ink droplets spread around these spots which increases the surface area of the drops. With a hotplate, the ink can be quickly dried. Once the first layer is dried, subsequent layers can be deposited on the dried ink to which the liquid adheres well. This laser treatment is suitable for larger and small scale actuators and fits the planar, additive manufacturing process.

Alternatively, plasma treatment can be used to improve the ink adhesion to the kapton substrate. Labiano et al. [9] manufactured graphene antennas on kapton. Here, the authors used plasma to improve the adhesion of graphene ink to the substrate. The graphene ink was deposited with an inkjet printer. However, this method was not effective for the spray-deposition machine. Contrary to an inkjet printer, the spray deposition machine uses air pressure to blow the ink droplets on the surface. The plasma treats the entire surface and as a result, the ink adheres to the designated area as well as

the undesired surrounding area. Therefore, the ink is still be blown across the surface before it dries out. It is possible to use masking, to create a hydrophobic barrier between plasma treated and untreated areas, as demonstrated by Khomiakove et al. [8]. However, masking might introduce problems when scaling down the size of the actuator, as the mask will need to be attached and removed in the correct location. Similarly, it will be difficult to attach the mask in the same position on both sides of the thin, flexible substrate. Thus, an alternative surface treatment method, which can more easily create a boundary between treated and untreated kapton, might be more suitable.

4) Printing process of bottom electrode: Now that a method is developed to deposit the electrode, we can characterize the resistivity of the electrode. This is done by measuring the sheet resistance of a set of samples for which we increase the amount of deposited layers. The sheet resistance is determined with a four-point probe [2]. The measurements were performed on samples containing one to 14 layers of spray deposited carbon ink and are shown in Fig. 8.

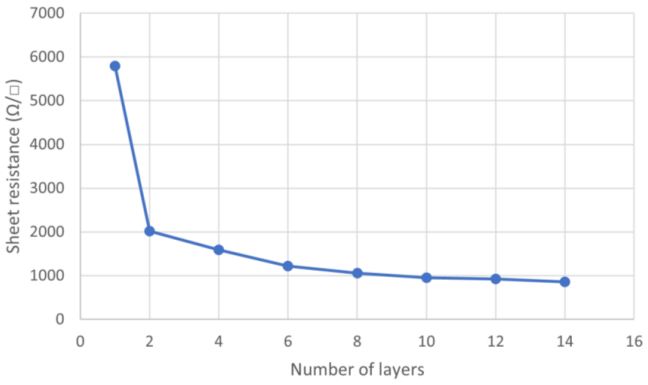

Fig. 8: Sheet resistance vs number of layers

The exact resistivity is dependent on the printing parameters and situational variables, such as deviations in pressure or temperature, and might fluctuate from the measured sheet resistance. A small decrease in pressure will deposit less ink and is likely to result in a higher resistivity for that layer. Similarly, situational variables such as room temperature and humidity, might result in comparable deviations. The graph does however provide some practical insights. Since each layer requires a certain printing time, it is advantageous to maximize the conductivity while minimizing the amount of layers. The experiments show that the sheet resistance does not significantly change after eight layers. Thus, the samples were manufactured with eight electrode layers.

5) Manufacturing limitations: The size of t and s as shown in Fig. 4, are limited by the manufacturing method. The spray deposition machine has a resolution of approximately 0.5mm [7]. Thus, to prevent connection between multiple fibres, s needs to be at least 1mm. Since we need to spray several layers, which will lower the spraying resolution, the spacing between fibres is taken as $s \geq 1.6$mm. Since we want thin electrodes, t is set at $0.5s$, or 0.8mm.

The design space of the spray deposition printer is limited to 55x55mm. To manufacture the actuator including the terminal to which the voltage source is connected within the design space, L$\leq$ 45mm. To actuate all diagonal lines, they need to be connected by a central voltage hub. The width of this hub is chosen to be the same width as s, 1.6mm. To ensure that a relatively large area of the actuator is dedicated to generating twisting deformation (the diagonal lines) with respect to supplying voltage, W is constrained at $W \geq 10$mm. This means the design does not fully satisfy the thin slender beam assumptions of the theoretical model in Subsec. II-A3 and thus, the predicted deformation will not be exact. However, we will consider the design slender enough to be compared to the model.

6) Manufacturing process: A schematic overview of the printing process is shown in Fig. 9. First, the kapton substrate is modified with a laser as discussed in Subsec. II-B3. Subsequently, the bottom electrodes, the EAP and the top electrode are spray deposited on the substrate in several layers. With experiments, the influence of all independent printing parameters were tested. These parameters are the needle retraction (flow rate allowed by airbrush), bed temperature (hot plate heating the substrate), the printing speed (movement speed of the airbrush in the manufacturing plane) and the air pressure (pushing the ink trough the airbrush). A parameter sweep from available research [7], is taken as guideline. The parameters are modified to adjust the flow rate of the ink trough the airbrush that is suitable for the smooth semi-hydrophobic nature of the kapton substrate. The deposition process is fine-tuned by varying the printing parameters to achieve a printing resolution capable of printing the 1.6mm design features from Fig. 4.

To ensure proper adhesion of the EAP to the electrodes, they need to be completely dry. This is achieved by heating the electrodes in an oven at 80°C for at least 12 hours. As described in Subsec. II-A2, a relatively thick layer of EAP is needed to prevent its dielectric breakdown under higher voltages. Since the bottom electrode is made up of eight layers, the EAP was doubled to 16 layers.

The final parameter combination shows a good resolution with homogeneous layers. In Table I the used parameters are shown that produced results with the desired printing resolution. While other combinations could lead to improvements, the set presented here are sufficient for a proof of concept.

After deposition of each of the three components, the samples are dried at 80°C for at least 12 hours. The sample is then annealed at 110°C for two hours. While depositing the layers of each material, the bed is heating the substrate to dry the layer's surface before the subsequent layers are deposited. Laser and deposition steps 1 to 4 are performed on both sides of the substrate to create a bimorph actuator.

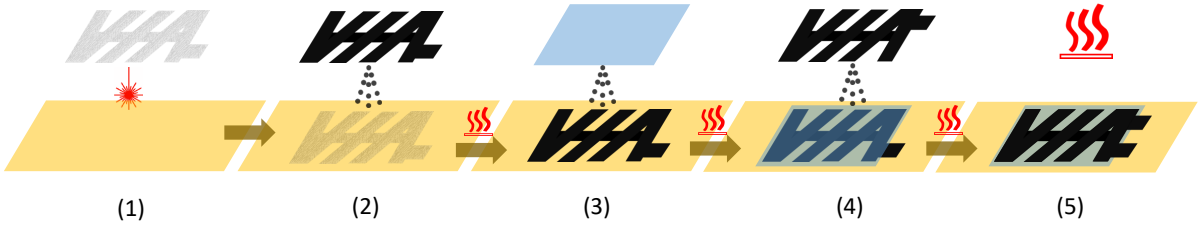

Fig. 9: Schematic overview of the manufacturing process

TABLE I: Final printing paramters

	Bot electrode		EAP	EAP*	Top electrode	
Layers	1-2	3-8	1-16	1-16	1-2	3-8
Needle retraction (*mm*)	-0.20	-0.20	-0.70	-0.60	-0.20	-0.20
Bed temperature (°C)	70	70	70	70	70	70
Printing speed (*mm/s*)	2500	2500	2500	2500	2500	2500
Pressure (psi)	18	21	23	21	18	21

* Settings used for thinner EAP layers, resulted in less consistent EAP deposition

C. Experimental setup

The samples are actuated using a waveform signal that is fed through an amplifier (MFC 1500/50). The displacement of the sample is measured using two lasers (OPTO NCDT1402, Micro-Epsilon), as shown in Fig. 10. The displacement of the two points on the sample are saved to a data acquisition card (USB-6211, Native Instruments). In a *LABVIEW* program which controls the setup, displacement measured by both laser 1 and 2, u_1 and u_2 respectively, is converted to a rotation of the sample according to Eq. 2.

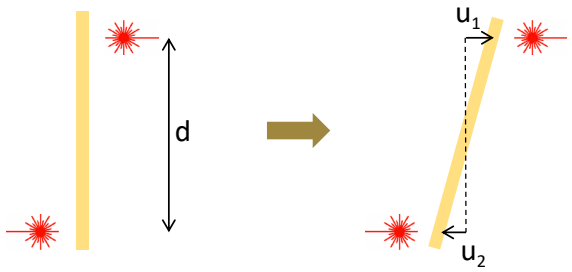

Fig. 10: Schematic overview of the measurement setup

$$\tau = arctan\left(\frac{u_1 + u_2}{d}\right) \tag{2}$$

Since the actuators are manufactured on a thin substrate, small internal stresses induced by the laser treatment or pretensioning of the substrate in the holder can result in permanent out-of-plane deformations. To ensure coherence between experiments, a small weight is clamped under the sample, see Fig. 11.

To prevent excitation of the sample around its resonant frequency, we measure its natural frequency. This is done by applying a small disturbance to one of the actuators and measuring its natural swinging and rotating frequency. All samples have the same length and mass. The clamped mass is significantly higher than the weight of the actuators. Thus, all samples will resemble a similar pendulum and thus have the same resonant frequency. Thus, all actuators will have a similar resonant frequency. The samples show a natural swinging and rotational frequency of 2Hz and 7-8Hz, respectively. Thus, the samples are actuated with a waveform with a frequency of 0.5Hz to avoid resonance.

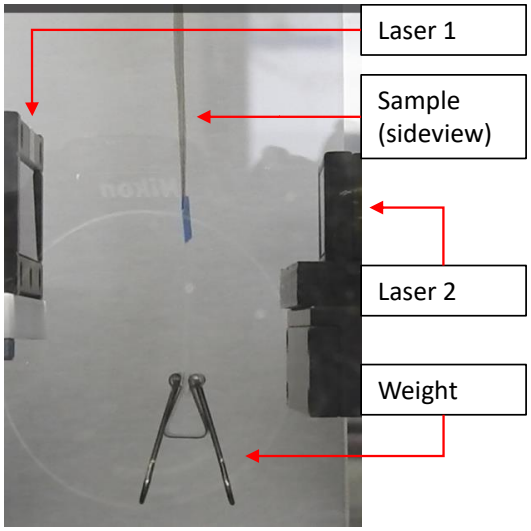

Fig. 11: Side view of the measurement setup

III. Results

In this section, an electrode pattern is generated from the methodology of Subsec. II-A2. With this pattern we manufacture four actuators according to Subsec. II-B6. The actuators have different widths, ranging from approximately 10 to 20mm as shown in Subsec. III-A. The actuators are examined using a scanning electron microscope (SEM). From the SEM, the thickness of the samples and all layers is measured. The twisting performance of the actuators with respect to the width

and thickness is experimentally analyzed in Subsec. III-B and Subsec. III-C, respectively.

A. Actuator samples

After considering the conceptual design and manufacturing limitations from Subsec. II-A2 and Subsec. II-B5 respectively, an electrode pattern is created. From Subsec. II-A3 we can recall that the *width* of the actuator was the most influential design parameter. Thus, from the design we generate the pattern with four different widths as shown in Fig. 12.

These designs are manufactured according to the methods described in Subsec. II-B6. One of the 20mm samples is shown in Fig. 13. After annealing, the samples are cut out of the holder and tested in the experimental setup.

With a scanning electron microscope (SEM), the cross-section of two different samples is analyzed. These 14mm wide samples are manufactured with a thick and thinn EAP layer according to Table I, see Fig. 14 and Fig. 15 respectively. All seven layers, as described in Fig. 5, are visible on the SEM image. From top to bottom in Fig. 14, one can see electrode, EAP, electrode, kapton, electrode, EAP and electrode. The printer settings for the manufacturing of the thin sample presented more issues than the thicker sample. During the manufacturing of the thinner EAP layer, more clogging in the airbrush was observed. In the SEM cross-sections it is seen that the EAP layers in the thin sample appears more porous than the EAP layers in the thicker sample.

B. Characterization of twisting performance with respect to the actuator width

The actuators have a thickness of approximately $139\mu m$ as measured with the SEM. With the width of the actuators from Fig. 12, we can find the expected twisting performance from Eq. 1, see Fig. 16. As discussed in Subsec. II-A3, we can merely qualify the amount of twisting. It is clearly shown that the rotation for the wider samples decays exponentially. Since the model assumes thin, slender beams, we expect the wider samples to not fit the model as well as the more slender samples. From Fig. 16 we can also see that the thickness of the actuator should have negligible influence on the magnitude of the twisting deformation.

The actuators are tested in the setup as described in Subsec. II-C. The samples are actuated for 30 seconds with a sinusoidal wave at a frequency of 0.5Hz. After ten seconds, the amplitude of the sinusoidal wave is incremented with 20 Volts, which is repeated till the samples break down. The results for the 10, 14, 17 and 20mm samples are shown in Fig. 17, Fig. 18, Fig. 19 and Fig. 20, respectively. In these figures, the electrode pattern is shown on the left, the entire experiment is shown in the center and the maximum rotation per Volt is shown on the right.

An overview is presented in Table II. The results of the experiments can be compared to Fig. 16 and we find an significant decay in rotation relative to the width of the sample in both the model and the experiments. From the experiments, we observe significant motion at the actuation frequency of 0.5Hz in both the 10 and 14mm sample. Similarly, these samples show a gradual increase in rotation when a higher voltage is applied. Both the 17 and 20mm sample show periodic motion at the actuation frequency, but only at very low magnitudes. I.e., these sample show little to no twisting with respect to the measured noise. The maximum rotation for the 17mm sample is taken from the oscillating actuation at 520V between 15s and 30s (green). This sample shows a semi-steady increase in rotation only between 420V and 520V. It is also found that the wider samples experience dielectric breakdown at higher voltages.

TABLE II: Experiment results

Sample	Max rotation [deg]	Breakdown [V]
10	2.29	250
14	0.678	480
17	$<$0.11*	540
20	-*	600

*Dominated by noise and external vibrations

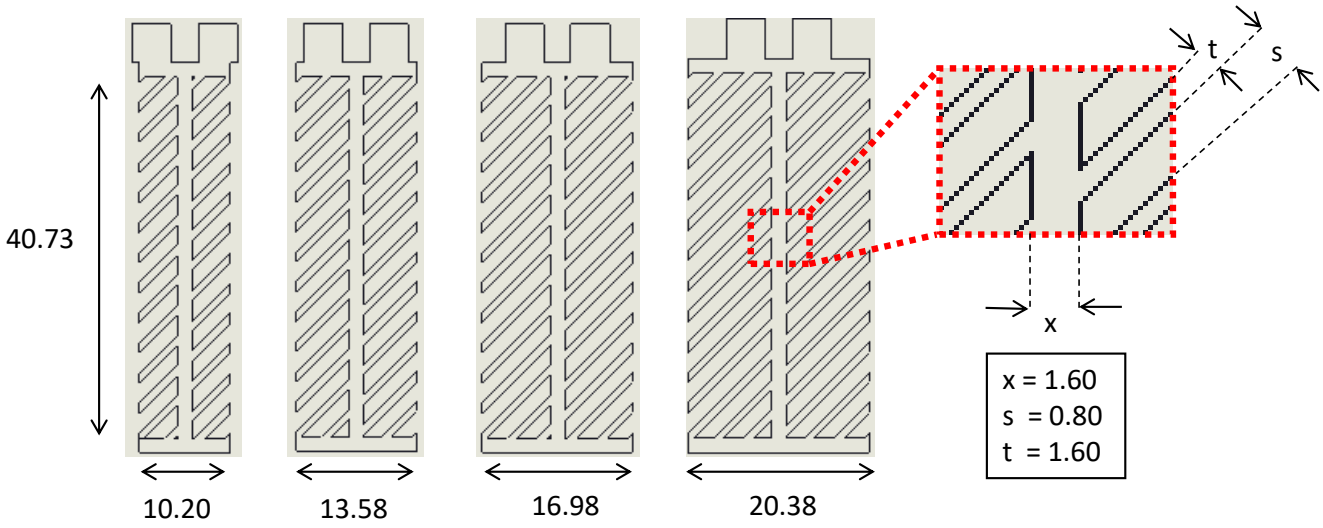

Fig. 12: Different electrode designs in mm. The designs are referred to from left to right as 10, 14, 17 and 20mm

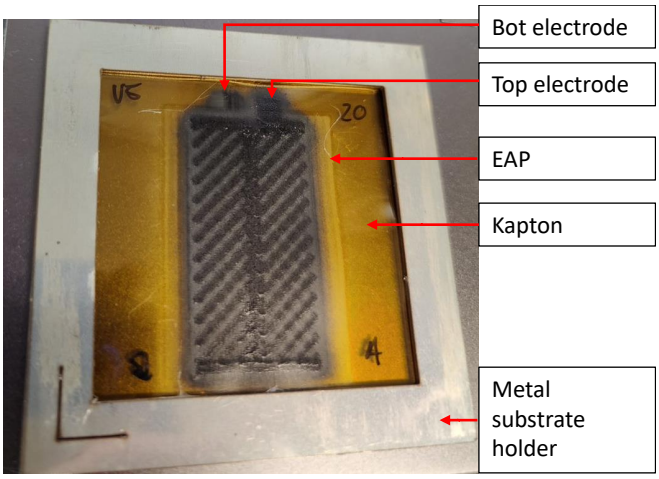

Fig. 13: 20mm actuator in sample holder

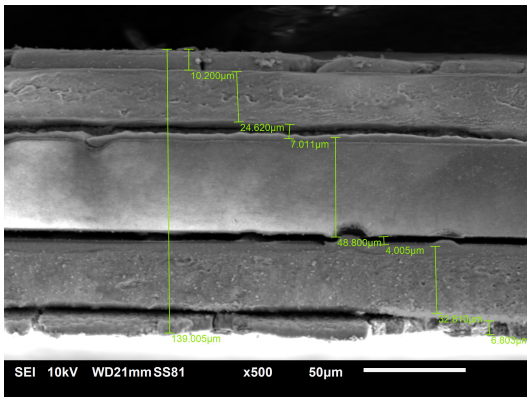

Fig. 14: SEM of cross-section of *thick* 14mm sample

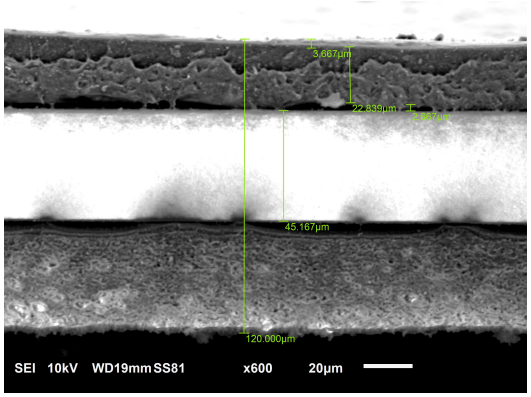

Fig. 15: SEM of cross-section of *thin* 14mm sample

C. Characterization of twisting performance with respect to the actuator thickness

In Fig. 16 it is shown how the effect of the thickness is negligible. However, this graph only considers the geometric parameters of the design. The thickness of the EAP has effect on the thickness of the overall design, but also on the strength of the electric field. A thinner EAP layer means the electrodes are closer together, thus a higher electric field is generated with a constant voltage. This will also influence the magnitude of the deformation, as shown in Eq. 1.

Both Fig. 14 and Fig. 15 are 14mm samples with a thickness of 139 and 120μm, respectively. The samples are actuated and the results are shown in Fig. 21 and Fig. 22. Comparing the two samples, we observe that the thinner sample produced 3.38° of rotation at 100V with respect to the thicker sample of 0.678° of rotation at 480V. This shows the thicker sample has significant less deformation but a much higher breakdown

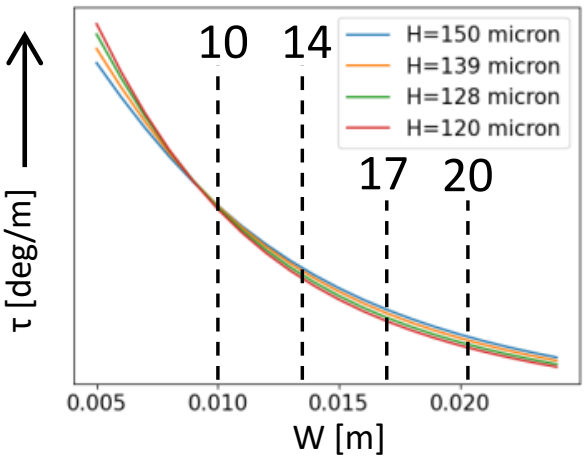

Fig. 16: Characterization of different W and H, where the dotted lines are the different electrode design widths from Fig. 12

voltage.

From Fig. 15 it is also found that the bottom EAP layer is significantly thicker than the top EAP layer. The cross section can be compared with Fig. 14, which is more symmetric. During the experiment, it is visually observed that the asymmetric, thinner sample exhibits a combination of bending and twisting deformation. Contrary, to the thicker sample, which shows more pure rotation. The thinner, uneven sample will experience higher actuation excitation in the top half of the actuator. As a result, the actuator will show unimorph bending behaviour in addition to the twisting deformations. Both the unimorph bending and bimorph twisting behaviour show up in the displacements measured by the two lasers. The two lasers in the experimental setup are measuring in opposite direction as shown in Fig. 10. In Fig. 24 it is found that Laser1 measures the sample coming closer to the laser source whereas Laser2 measures the sample moving away from the laser source. Thus, the sample shows a (unimorph) bending displacement of approximately 1.5mm. However, when evaluating at the relative difference in the measured displacements there is approximately three degrees of rotation. Similarly, Fig. 23 shows that both lasers are measuring the sample moving towards the source, i.e. pure rotation. Thus, the symmetry of the samples has a large influence on the performance of the actuator.

The uneven EAP deposition might also explain the negative rotations that are measured. When one layer or small, local areas in a layer are thinner, the sample can deform in unexpected manners. If the two areas on the sample where the lasers measure both move away from the source, this is interpreted as a negative rotation. These negative rotations only occur between 0 and -0.35°.

From SEM images Fig. 14 and Fig. 15 it is concluded that thinner samples have a more porous (grainy) cross-section than thicker samples. It is possible that the porosity of the sample caused the thinner sample to experience dielectric breakdown at a lower voltage. Since all samples were manufactured at different times, the variations in porosity can be explained by a different temperature or humidity in the manufacturing setup. It is also possible, that the difference is caused by the manufacturing process itself, although both samples were manufactured with the printing parameters as shown in Table I. The 16 EAP layers for the thicker samples were deposited in two steps. First, eight layers on the top side of the substrate and then eight layers on the bottom side before adding layers 9 to 16. This gave the EAP around 10 minutes of drying between the deposition of the two sets of 8 layers. Since the thinner samples where produced with different settings, the process was more prone to clogging up the airbrush. Therefore, the EAP was deposited only two layers at the time. Between each two layers, the airbrush had to be flushed with acetone to remove any clogs. It is possible that small clogs or the drying of the layers while removing the clogs, influenced the quality of the EAP layer. However, this was not investigated in this study.

IV. Discussion

This study presents a design methodology to develop a bimorph piezoelectric twisting actuator. To the author's best knowledge, this was not yet experimentally studied before this study. These actuators show a fast response where maximum deformation is reached in approximately five seconds. Other smart material twisting actuators use shape memory alloys to deform, which takes up to 102.4 seconds to achieve maximum deformation. The fast response is a trade-off with the maximum achievable deformation. The piezoelectric actuator is measured to have up to 3.38° of rotation contrary to the shape memory alloy actuator that rotates around 100°. This trade-off was predicted by literature. This study was done as a proof of concept, thus it is plausible that optimization of the design parameters and the manufacturing process will lead to larger deformations for piezoelectric twisting actuators. In the experiments, the actuators were loaded with a mass. It is not yet investigated how much this load influenced the deformation with respect to an unloaded actuator.

Theory shows that the thickness of the actuator has negligible influence on the twisting performance. However, experiments show that the thickness off the EAP layer can have significant influence on the magnitude of the applied electric field. The model that was used [1], uses a stimulating electric field along the direction of piezoelectric fibres. Thus, the modelled d_{33} actuation is not dependent on the thickness of the actuator. The d_{31} deformation of the EAP used in this study, deforms as a function of E^2. A thinner EAP layer will have the electrode layers closer together which generates a stronger electric field at a constant voltage. Thus, a thicker EAP will quadratically decrease the magnitude of the deformations.

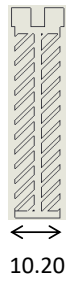

(a)

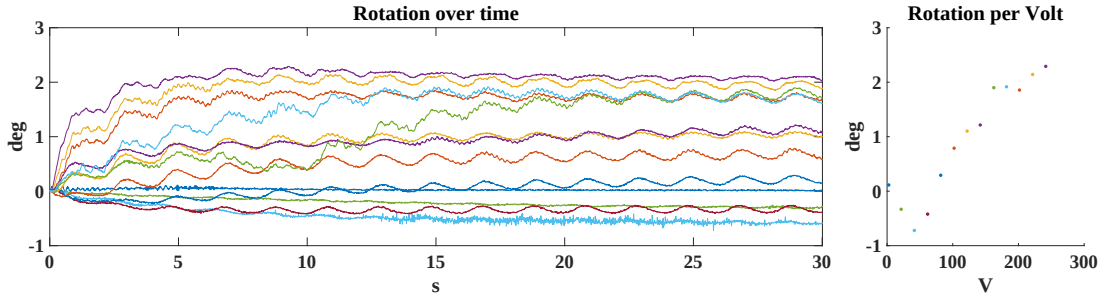

(b)

Fig. 17: 10mm sample, breakdown after 250V

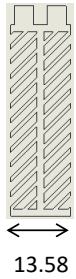

(a)

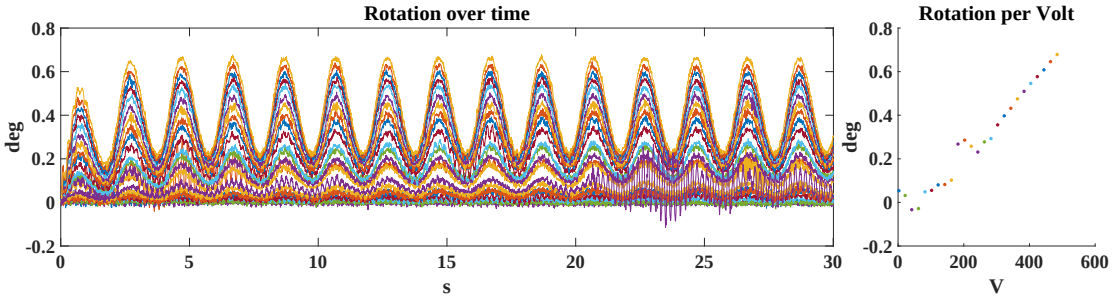

(b)

Fig. 18: 14mm sample, breakdown after 480V

(a)

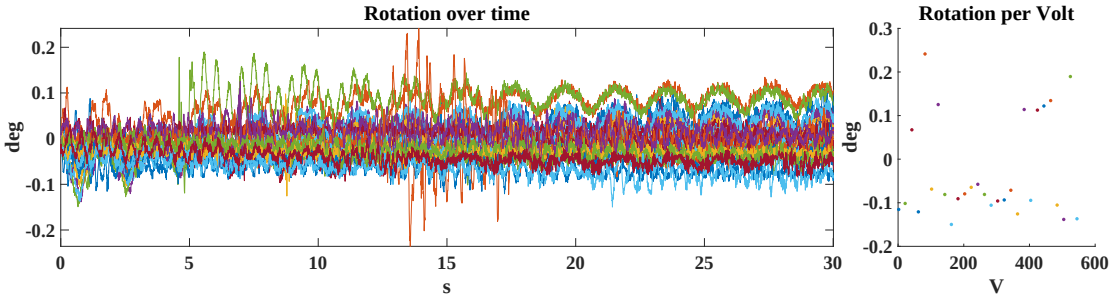

(b)

Fig. 19: 17mm sample, breakdown after 540V

(a)

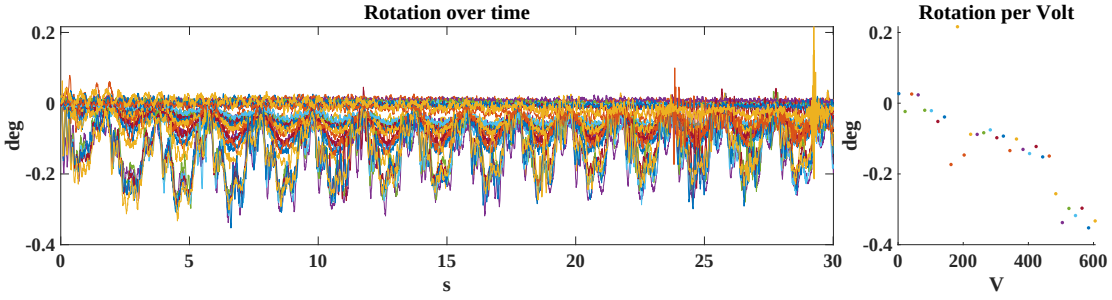

(b)

Fig. 20: 20mm sample, breakdown after 600V

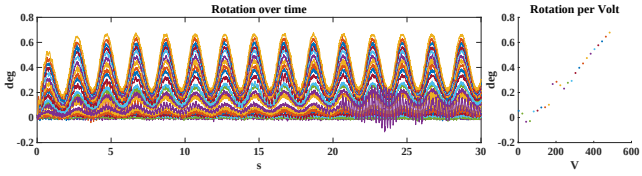

Fig. 21: *Thick* 14mm sample, breakdown after 400V

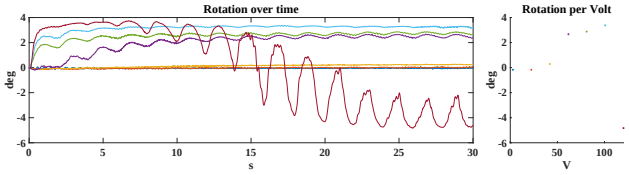

Fig. 22: *Thin* 14mm sample, breakdown after 100V

SEM analysis of the different samples show that thinner samples have more porous EAP layers than thicker samples. It is theorized that the porosity in introduced in the manufacturing process, as the production of the thinner samples was more prone to airbrush clogging. However, this is not investigated further.

The thinner samples show dielectric breakdown at lower voltages. It is possible that this breakdown happens more easily due to the porosity of the EAP layers. Another possibility is that the dielectric breakdown happens at lower voltages when larger deformations are induced. It is observed that the more slender samples show more rotation but break down at lower voltages. Large deformations might induce cracks, or create thin localized areas where dielectric breakdown can occur. It is also possible that the actuators simply fail at lower voltages because the EAP layer is thinner. A thinner EAP will induce a larger electric field at a constant voltage as the electrodes are closer together. It is uncertain which factors have most influence on the dielectric breakdown performance of the actuators.

In the experiments, we observe that some actuators show pure bimorph twisting while other actuators show unimorph bending behaviour in addition to rotation. The SEM images show that some samples have uneven top and bottom EAP layers. This thicker layer will be stimulated by a lower electric field than the thinner layer. As a result, the thinner layer will deform more than the thicker layer. The effect of asymmetric layers in the actuators is also measured with the lasers in the experimental setup. Thus the performance, i.e. pure rotation or rotation and bending, of the actuator is dependent on the consistency of the spray-deposition process.

V. Conclusion

This study successfully designs, manufactures and experimentally identifies the twisting performance of, to the author's best knowledge, the first bimorph piezoelectric actuators. From a model on the deformation of piezoelectric macro fibre composites [1], a methodology is developed to generate out-

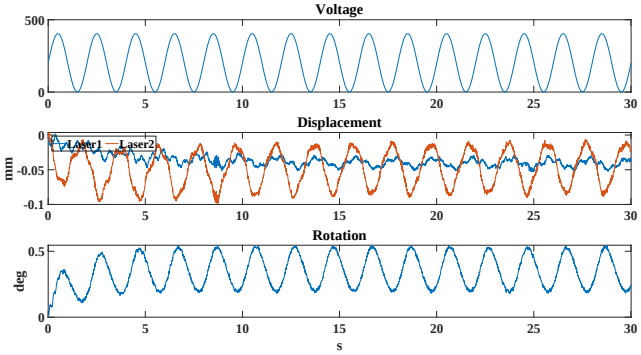

Fig. 23: *Thick* 14mm sample, actuation at 400V

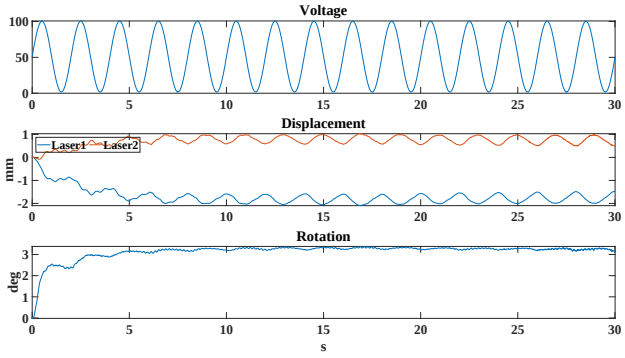

Fig. 24: *Thin* 14mm sample, actuation at 100V

of-plane rotation. We demonstrate how an electrode with thin diagonal features can selectively stimulate parts of an EAP layer to achieve the desired deformation. With this concept, we create actuators with a width of 10, 14, 17 and 20mm and a length of 41mm. A spray-deposition platform is modified to enable the manufacturing of the bimorph design. The actuators are built up of P(VDF-TrFE- CTFE) polymer for the actuation and Carbon Black (JR-700HV) electrodes on a kapton substrate. The actuators have a thickness of approximately 139μm. We measure maximum rotation of 3.38° in a 14mm actuator with a thickness of 120μm. This sample broke down at 100V. Actuators with a thickness of approximately 139μm and width of 10, 14 and 17mm have a maximum rotation of 2.29, 0.678 and 0.11 degrees, respectively. The experiments also show that these samples have dielectric breakdown of 250, 480 and 540V, respectively. The experiments show that the samples exhibit pure twisting, for symmetric cross-sections. For asymmetric cross-sections, the actuators show a combination of bimorph twisting and unimorph bending. In this study, we identify several factors that influence the dielectric breakdown of the actuators which are recommended to study in future work. These factors are the porosity of the EAP layers, the thickness of the EAP layers and the magnitude of the deformation. With current experiments, it is uncertain which factor is most influential

for the breakdown of the actuators. Further development of these actuators can be done by increasing the consistency and porosity over the P(VDF-TrFE- CTFE) layers. Similarly, we recommend to investigate how larger deformations might introduce cracks, or thin spots where the actuators can break down. This study merely investigated the magnitude of the deformation, and we suggest to identify the force displacement characteristics of these actuators.

REFERENCES

[1] Jagannadh Boddapati, Shaswat Mohanty, and Ratna Kumar Annabattula. "An analytical model for shape morphing through combined bending and twisting in piezo composites". In: *Mechanics of Materials* 144 (May 2020), p. 103350. ISSN: 01676636. DOI: 10.1016/j.mechmat.2020.103350.

[2] *Calculate Sheet Resistance Using the Four-Probe Method*. https://www.ossila.com/en-eu/pages/sheet-resistance-theory.

[3] Amir Firouzeh et al. "Sensor and actuator integrated low-profile robotic origami". In: IEEE, Nov. 2013, pp. 4937–4944. ISBN: 978-1-4673-6358-7. DOI: 10.1109/IROS.2013.6697069.

[4] Mahpara Habib, Iza Lantgios, and Katherine Hornbostel. "A review of ceramic, polymer and composite piezoelectric materials". In: *Journal of Physics D: Applied Physics* 55 (42 Oct. 2022), p. 423002. ISSN: 0022-3727. DOI: 10.1088/1361-6463/ac8687.

[5] E. Hawkes et al. "Programmable matter by folding". In: *Proceedings of the National Academy of Sciences* 107 (28 July 2010), pp. 12441–12445. ISSN: 0027-8424. DOI: 10.1073/pnas.0914069107.

[6] Ahmed Olanrewaju Ijaola et al. "Wettability Transition for Laser Textured Surfaces: A Comprehensive Review". In: *Surfaces and Interfaces* 21 (Dec. 2020), p. 100802. ISSN: 24680230. DOI: 10.1016/j.surfin.2020.100802.

[7] Stijn IJssel de Schepper and Andres Hunt. "An Airbrush 3d Printer: Additive Manufacturing of Relaxor Ferroelectric Actuators". In: *Available at SSRN 4558463* ().

[8] Natalia Khomiakova et al. "Investigation of Wettability, Drying and Water Condensation on Polyimide (Kapton) Films Treated by Atmospheric Pressure Air Dielectric Barrier Discharge". In: *Coatings* 10 (7 June 2020), p. 619. ISSN: 2079-6412. DOI: 10.3390/coatings10070619.

[9] Isidoro Ibanez Labiano and Akram Alomainy. "Flexible inkjet-printed graphene antenna on Kapton". In: *Flexible and Printed Electronics* 6 (2 June 2021), p. 025010. ISSN: 2058-8585. DOI: 10.1088/2058-8585/ac0ac1.

[10] Su-Yeon Lee and Gil-Yong Lee. "Largely deformable torsional soft morphing actuator created by twisted shape memory alloy wire and its application to a soft morphing wing". In: *Scientific Reports* 13 (1 Oct. 2023), p. 17629. ISSN: 2045-2322. DOI: 10.1038/s41598-023-44936-4.

[11] Nuri Park and Jaeyun Kim. "Hydrogel-Based Artificial Muscles: Overview and Recent Progress". In: *Advanced Intelligent Systems* 2 (4 Apr. 2020), p. 1900135. ISSN: 2640-4567. DOI: 10.1002/aisy.201900135.

[12] Shashank Sarbada and Yung C. Shin. "Superhydrophobic contoured surfaces created on metal and polymer using a femtosecond laser". In: *Applied Surface Science* 405 (May 2017), pp. 465–475. ISSN: 01694332. DOI: 10.1016/j.apsusc.2017.02.019.

[13] A Singh et al. "Extreme on-demand contactless modulation of elastic properties in magnetostrictive lattices". In: *Smart Materials and Structures* 31 (12 Dec. 2022), p. 125005. ISSN: 0964-1726. DOI: 10.1088/1361-665X/ac9cac.

[14] David C. Stanier, Jacopo Ciambella, and Sameer S. Rahatekar. "Fabrication and characterisation of short fibre reinforced elastomer composites for bending and twisting magnetic actuation". In: *Composites Part A: Applied Science and Manufacturing* 91 (Dec. 2016), pp. 168–176. ISSN: 1359835X. DOI: 10.1016/j.compositesa.2016.10.001.

[15] *TECHNICAL GUIDE PIEZOTECH® RT-TS*. https://piezotech.arkema.com/en/Products/high-k-terpolymers/. 2020.

[16] N. Torras et al. "Bending kinetics of a photo-actuating nematic elastomer cantilever". In: *Applied Physics Letters* 99 (25 Dec. 2011), p. 254102. ISSN: 0003-6951. DOI: 10.1063/1.3670502.

4 Conclusion

In this study a group of planar mechanisms is identified that can comply with out-of-plane motion; *lamina emergent mechanisms (LEMs)*. To do so, LEMs are composed of elements that support and comply with out-of-plane bending or twisting motions. By embedding smart materials within these mechanisms, we can develop small scale actuators capable of generating complex 3D motion. It is found that many smart materials are capable generating bending motion, but twisting deformations are underdeveloped. Thus, a bimorph piezoelectric twisting actuator is developed. To the author's best knowledge, this is the first fast response smart material twisting actuator. From a model on the deformation of piezoelectric macro fibre composites, a methodology is developed to generate out-of-plane rotation. We demonstrate how an electrode with thin diagonal features can selectively stimulate parts of an EAP layer to achieve the desired deformation. With this concept, we create actuators with a width of 10, 14, 17 and 20mm and a length of 41mm. A spray-deposition platform is modified to enable the manufacturing of the bimorph design. The actuators are built up of P(VDF-TrFE- CTFE) polymer for the actuation and Carbon Black (JR-700HV) electrodes on a kapton substrate. The actuators have a thickness of approximately 139μm. We measure maximum rotation of 3.38° in a 14mm actuator with a thickness of 120μm. This sample broke down at 100V. Actuators with a thickness of approximately 139μm and width of 10, 14 and 17mm have a maximum rotation of 2.29, 0.678 and 0.11 degrees, respectively. The experiments also show that these samples have dielectric breakdown of 250, 480 and 540V, respectively. The experiments show that the samples exhibit pure twisting, for symmetric cross-sections. For asymmetric cross-sections, the actuators show a combination of bimorph twisting and unimorph bending. In this study, we identify several factors that influence the dielectric breakdown of the actuators which are recommended to study in future work. These factors are the porosity of the EAP layers, the thickness of the EAP layers and the magnitude of the deformation.

5 Appendix

Here, fileguide is presented. The files are available per request. Please contact:

- T.A. Baaij (author)
- Dr. ir. L.F.P Noël (supervisor)
- Dr. ir. A. Hunt (supervisor)

1. Printer Modification
   (a) Solidworks files for metal substrate holder
2. Inkscape
   (a) Test print and printer calibration files
   (b) Sample holder (design space)
   (c) Sample designs
   (d) Inkscape code and instructions
3. Experiments
   (a) Videos
   (b) Code to run experimental setup
   (c) Experimental data